Article

Neuron

Drd3 Signaling in the Lateral Septum Mediates Early Life Stress-Induced Social Dysfunction

Highlights

- Early social deprivation (ESD) causes downregulation of Drd3 signaling in the LS
- Blunted LS Drd3 neuronal activity mediate ESD-induced social dysfunctions
- Drd3 signaling has corresponding effects on neuronal activity in the LS
- Activation of Drd3 signaling in the LS normalize social impairments of ESD mice

Authors

Sora Shin, Horia Pribiag, Varoth Lilascharoen, Daniel Knowland, Xiao-Yun Wang, Byung Kook Lim

Correspondence

bklim@ucsd.edu

In Brief

Exposure to early adverse experiences is associated with an increased risk of developing social dysfunction later in life. Shin et al. show that Drd3 signaling and its corresponding effects on neural activity in the LS are both necessary and sufficient to cause early life stress-induced social abnormalities in adulthood.

Shin et al., 2018, Neuron *97*, 195–208
January 3, 2018
https://doi.org/10.1016/j.neuron.2017.11.040

CellPress

Neuron
Article

Drd3 Signaling in the Lateral Septum Mediates Early Life Stress-Induced Social Dysfunction

Sora Shin,[1] Horia Pribiag,[1] Varoth Lilascharoen,[1] Daniel Knowland,[2] Xiao-Yun Wang,[1] and Byung Kook Lim[1,2,3,4,*]
[1]Neurobiology Section, Division of Biological Sciences, University of California, San Diego, La Jolla, CA 92093, USA
[2]Neurosciences Graduate Program, University of California, San Diego, La Jolla, CA 92093, USA
[3]Biomedical Sciences Graduate Program, University of California, San Diego, La Jolla, CA 92093, USA
[4]Lead Contact
*Correspondence: bklim@ucsd.edu
https://doi.org/10.1016/j.neuron.2017.11.040

SUMMARY

Early life stress (ELS) in the form of child abuse/neglect is associated with an increased risk of developing social dysfunction in adulthood. Little is known, however, about the neural substrates or the neuromodulatory signaling that govern ELS-induced social dysfunction. Here, we show that ELS-induced downregulation of dopamine receptor 3 (Drd3) signaling and its corresponding effects on neural activity in the lateral septum (LS) are both necessary and sufficient to cause social abnormalities in adulthood. Using *in vivo* Ca^{2+} imaging, we found that Drd3-expressing-LS ($Drd3^{LS}$) neurons in animals exposed to ELS show blunted activity in response to social stimuli. In addition, optogenetic activation of $Drd3^{LS}$ neurons rescues ELS-induced social impairments. Furthermore, pharmacological treatment with a Drd3 agonist, which increases $Drd3^{LS}$ neuronal activity, normalizes the social dysfunctions of ELS mice. Thus, we identify Drd3 in the LS as a critical mediator and potential therapeutic target for the social abnormalities caused by ELS.

INTRODUCTION

Children exposed to early life stress (ELS) such as physical abuse and emotional neglect during a critical period in their development are more likely to display social dysfunction later in life (Bandelow et al., 2004; Heim and Nemeroff, 2001; Kessler et al., 1997). Symptoms of disrupted social behaviors include decreased social motivation and a lack of interest in attending to social stimuli or seeking and enjoying reciprocal social interactions (Kohls et al., 2013). Given that high levels of early adversity are also associated with the asocial behaviors of psychiatric patients (Bolger and Patterson, 2001), identifying the neural mechanisms underlying ELS-induced social dysfunction is essential for the development of treatment strategies for mental illnesses associated with social impairments, such as autism spectrum disorder (ASD) (Rai et al., 2012), schizophrenia (Agid et al., 1999), and major depressive disorder (MDD) (Kendler et al., 1999).

Moreover, clinical studies have suggested that MDD patients with a history of ELS exhibit significantly poorer responses and lower remission rates upon receiving conventional pharmacotherapy and psychotherapy (Bruce et al., 2012; Nanni et al., 2012). This suggests that such individuals possess a distinct endophenotype that will require alternative therapeutic strategies (Nemeroff, 2016). In this context, several recent studies have addressed the neurobiological characteristics of individuals exposed to ELS by pointing to putative dysfunctions in reward-related brain activation (Goff et al., 2013). For example, blunted reactivity to rewarding stimuli in the ventral striatum of adult participants with a history of ELS may constitute a neural mechanism by which ELS increases the risk of many psychiatric symptoms in adulthood (Hanson et al., 2016). However, neither the specific neural substrates nor the precise neuromodulatory mechanisms that transduce ELS into altered neuronal activity resulting in social dysfunction in adulthood are well understood. Thus, the identification of the specific neural mechanisms underlying ELS-induced social abnormalities is a critical next step for the development of therapeutics for psychiatric diseases elicited by ELS.

The lateral septum (LS) is thought to be critical for processing emotional information and for modulating behavioral responses to stress (Guzmán et al., 2013; Sheehan et al., 2004; Singewald et al., 2011). Moreover, the LS has been identified as a potent site for electrical self-stimulation in both rodents and humans (Heath, 1963; Olds and Milner, 1954), and it also has been implicated in reward-related processes such as drug addiction and social behaviors (Harasta et al., 2015; Luo et al., 2011; Mesic et al., 2015). Notably, the LS receives dopaminergic inputs from the ventral tegmental area (VTA) (Reddy et al., 2016)—a critical component of the reward circuitry—and contains subpopulations of neurons that express dopamine receptors that have not yet been subjected to functional dissection.

Here, we identify dopamine receptor 3 (Drd3)-expressing-LS ($Drd3^{LS}$) neurons as a critical component mediating the detrimental effects of ELS on social behavior. Employing an early social deprivation (ESD) stress paradigm, we found that Drd3 signaling in the LS is significantly downregulated in mice exposed to ESD and that this is accompanied by abnormal social behaviors such as reduced social preferences and severe communication deficits. Furthermore, the $Drd3^{LS}$ neurons of ESD mice show significantly decreased reactivity to social stimuli, while their optogenetic activation ameliorates ESD-induced

social impairment. Notably, pharmacological treatment with the Drd3 agonist PD128907, which increases Drd3^{LS} neuron activity, normalizes the abnormal social behaviors of ESD mice. Simultaneous knockdown of Drd3 in the LS, however, abolishes this pharmacological rescue. Taken together, our findings identify Drd3^{LS} neuronal signaling as a critical mediator of the ELS-induced social impairments in adulthood. Drd3 in the LS may therefore constitute an important therapeutic target for the treatment of the severe social impairments commonly observed in numerous neuropsychiatric disorders.

RESULTS

Adult ESD Mice Display Social Dysfunction and Reduced c-*fos* Induction in the LS in Response to Social Stimuli

To investigate how ELS affects social behavior later in life, we adopted the ESD stress paradigm that disrupts early social bonding by exposing pups to daily infant-mother/littermate separation during their first 2 weeks of postnatal life (Figures 1A and 1B; see STAR Methods). Adult mice (8–12 weeks old) exposed to ESD showed no significant differences from controls in locomotion, anxiety-like behaviors, novel object recognition, or olfactory perception (Figures S1A–S1F).

We first compared ESD and control mice using the three-chamber social preference test. This test quantifies a mouse's preference for investigating a novel mouse versus an object; it has been used to measure social defects in mouse models of psychiatric disorders that present with social dysfunction (Silverman et al., 2010). In test sessions, ESD mice showed significantly reduced social preference for a stranger mouse over an object compared to control mice, whereas, in habituation sessions, both control and ESD mice showed no preference for the two sides of the three-chambered arena (Figures 1C–1E, S1G, and S1H). We also found that ESD mice exhibited a profound defect in direct social contacts in a reciprocal social interaction test (Figures 1F and 1G). To further explore the social impairments of ESD mice, we measured their ultrasonic vocalizations (USVs) (Jamain et al., 2008). Upon encountering a female, male ESD mice produced significantly fewer calls and show higher latency to their first call than control mice, indicating that ESD mice have defective social communication (Figures 1H–1J).

To identify specific brain regions that contribute to ESD-induced social dysfunction, we quantified the expression of the neuronal activation marker c-*fos* across several brain regions in response to social stimuli (Figure 1K). Using immunohistochemistry, we found that, after exposing control mice to social stimuli, they showed significant increases in c-*fos* expression in the LS, but ESD mice did not (Figures 1L and 1M). Notably, control mice showed the largest c-*fos* induction in the rostral LS rather than the caudal LS (Figures S2A–S2C). We also observed reliable differences in c-*fos* induction in the VTA of control mice but no distinguishable changes in the medial prefrontal cortex (mPFC), nucleus accumbens (NAc), ventral pallidum (VP), anterior hypothalamus (AHA), or lateral hypothalamus (LH) (Figures S2D–S2I).

Together, these results indicate that ESD stress can induce social dysfunctions in adulthood and that activity in the rostral part of the LS may play a critical role in regulating these processes.

Drd3 Signaling Is Downregulated in the LS Following ESD Stress Exposure

Previous reports indicated that the LS contains heterogeneous cell types, with each expressing different receptors for neuromodulators that regulate social behaviors (Mesic et al., 2015; Risold and Swanson, 1997). It remains unclear, however, how exposure to early adversity affects neuromodulatory signaling through specific receptors in the LS to produce psychiatric symptoms such as asocial behaviors. We therefore examined what molecular signaling in the LS may be altered by ESD stress and whether such changes mediate a disruption of normal social behaviors in adulthood. Using quantitative real-time PCR, we found that ESD mice showed lower Drd3 mRNA expression in the LS compared to control mice. We did not observe any changes for receptors of other neuromodulators including serotonin, oxytocin, glutamate, or glucagon (Figure 2A).

Drd3, a member of the D2-like receptor family, has been implicated in the development of social deficits associated with ASD (Staal et al., 2015), but its precise roles in mediating social abnormalities following ELS and in regulating neuronal activity in the LS are unknown. Thus, to investigate this, we used Drd3::Cre bacterial artificial chromosome (BAC) transgenic mice, which enable genetic manipulation of Drd3^{LS} neurons. Using dual fluorescent *in situ* hybridization (FISH), we confirmed that Drd3::Cre mice express Cre recombinase specifically in Drd3^{LS} neurons (Figure 2B). Consistent with previous studies (Zhao et al., 2013), we found that Drd3^{LS} neurons are predominantly GABAergic (Figure 2C). Intriguingly, Drd3::Cre mice crossed with the Ai6 reporter mice line revealed the most prominent Drd3 expression in the rostral part of LS. We then further confirmed this in wild-type mice using quantitative real-time PCR (Figures 2D and 2E). This suggests that Drd3^{LS} neurons may be responsible for the social stimulus-induced c-*fos* expression that we observed in the rostral LS (Figures S2A–S2C).

To further explore the function of the Drd3^{LS} neurons in social behavior, we asked whether the social stimulus-induced expression of c-*fos* we observed is occurring in Drd3^{LS} neurons. We injected adeno-associated virus (AAV) expressing the Cre-dependent eGFP (AAV-DIO-eGFP) into the LS of control Drd3::Cre mice to visualize Drd3^{LS} neuronal cell bodies. We then measured the proportion of c-*fos*-positive cells among eGFP-expressing neurons in the LS. We found that social stimulation enhances c-*fos* expression in the Drd3^{LS} neuronal population by up to 47.6% (Figures 2F–2H). Conversely, we observed that 50.42% of social stimulus-induced c-*fos* expression were overlapped with eGFP-expressing cells (data not shown), suggesting that Drd3^{LS} neurons constitute a relevant population preferentially activated by social stimuli (Figures 2F–2H).

To gain a holistic understanding of how Drd3^{LS} neurons contribute to ESD-induced abnormal social behaviors, we next aimed to delineate the circuitry of the Drd3^{LS} neurons. To this end, we injected the LS of wild-type mice with AAV expressing eGFP (AAV-eGFP) or the LS of Drd3::Cre mice with AAV-DIO-eGFP. While LS neurons in general project to the medial preoptic area (MPA), AHA, LH, VTA, and periaqueductal gray (PAG),

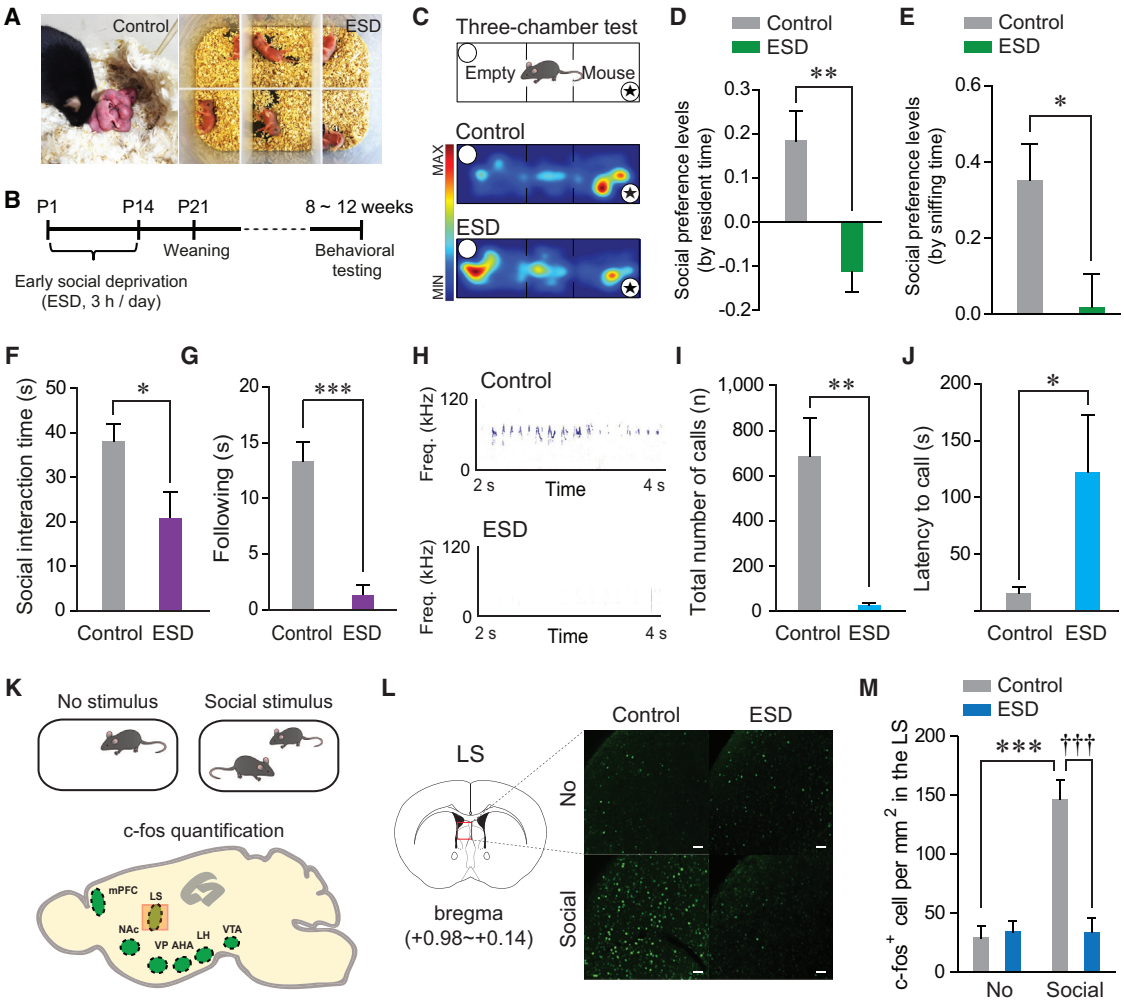

Figure 1. ESD Mice Exhibit Impaired Social Behaviors and Reduced c-*fos* Expression in the LS in Response to Social Stimuli

(A) Control pups remained with their dam (left), but ESD pups were removed and separated both from their dam and littermates (right).

(B) The experimental timeline for the ESD stress procedure.

(C) Schematic illustrating the three-chamber social preference test (top) and representative heatmap images during the test session for control (middle) and ESD (bottom) mice. Asterisks indicate the presence of a conspecific stranger.

(D and E) Social preference levels based on resident time (D) and sniffing time (E) in the three-chamber test. ESD mice showed significantly reduced preference for exploring a stranger mouse (n = 7, 11 mice per group).

(F and G) Reciprocal social interaction tests. ESD mice exhibited reduced total duration of direct contacts with a freely moving stranger mouse, as measured by amount of time spent in social interactions (i.e., sniffing, following, mounting, and nose to nose contacts) (F), and in following only (G) (n = 6 mice per group).

(H) Representative images of USVs produced by a control (top) and ESD (bottom) male mouse encountering a female mouse.

(I and J) ESD mice emitted significantly fewer USVs (I) and showed delayed latency to the first USV call (J) compared to controls (n = 12, 7 mice per group).

(K) c-*fos* expression was examined at baseline (no stimulus) or after social interactions (top). Brain schematic illustrating the target areas analyzed for c-*fos* quantification (bottom). mPFC, medial prefrontal cortex; NAc, nucleus accumbens; VP, ventral pallidum; AHA, anterior hypothalamus; LH, lateral hypothalamus; VTA, ventral tegmental area.

(L) Representative images of the LS showing c-*fos* staining in control versus ESD mice following exposure to a social stimulus. Scale bars, 50 μm.

(M) Quantification of c-*fos*-positive cells in the LS. Social stimuli elicited robust increases in c-*fos* expression within the LS of control, but not ESD mice (n = 6 mice for each no stimulus group and n = 7 mice for each social stimulus group).

Significance for multiple comparisons: unpaired t test (D–G), Mann-Whitney U test (I and J), and two-way ANOVA, post hoc, Bonferroni (M), *$p < 0.05$; **$p < 0.01$; ***$p < 0.001$; $^{\dagger\dagger\dagger}p < 0.001$. Data are expressed as mean ± SEM.

See also Figures S1 and S2.

among other areas, Drd3^{LS} neurons project specifically to the MPA, AHA, and LH (Figures S3A–S3M). Using viral expression strategies that reveal monosynaptic inputs (Figures S3N–S3S) (Callaway and Luo, 2015), we found that Drd3^{LS} neurons receive synaptic inputs from the MPA and AHA, as well as the ventral hippocampus and VTA (Figures S3T–S3Y). These data indicate that Drd3^{LS} neurons are directly connected to several brain areas known to be implicated in the regulation of social behaviors

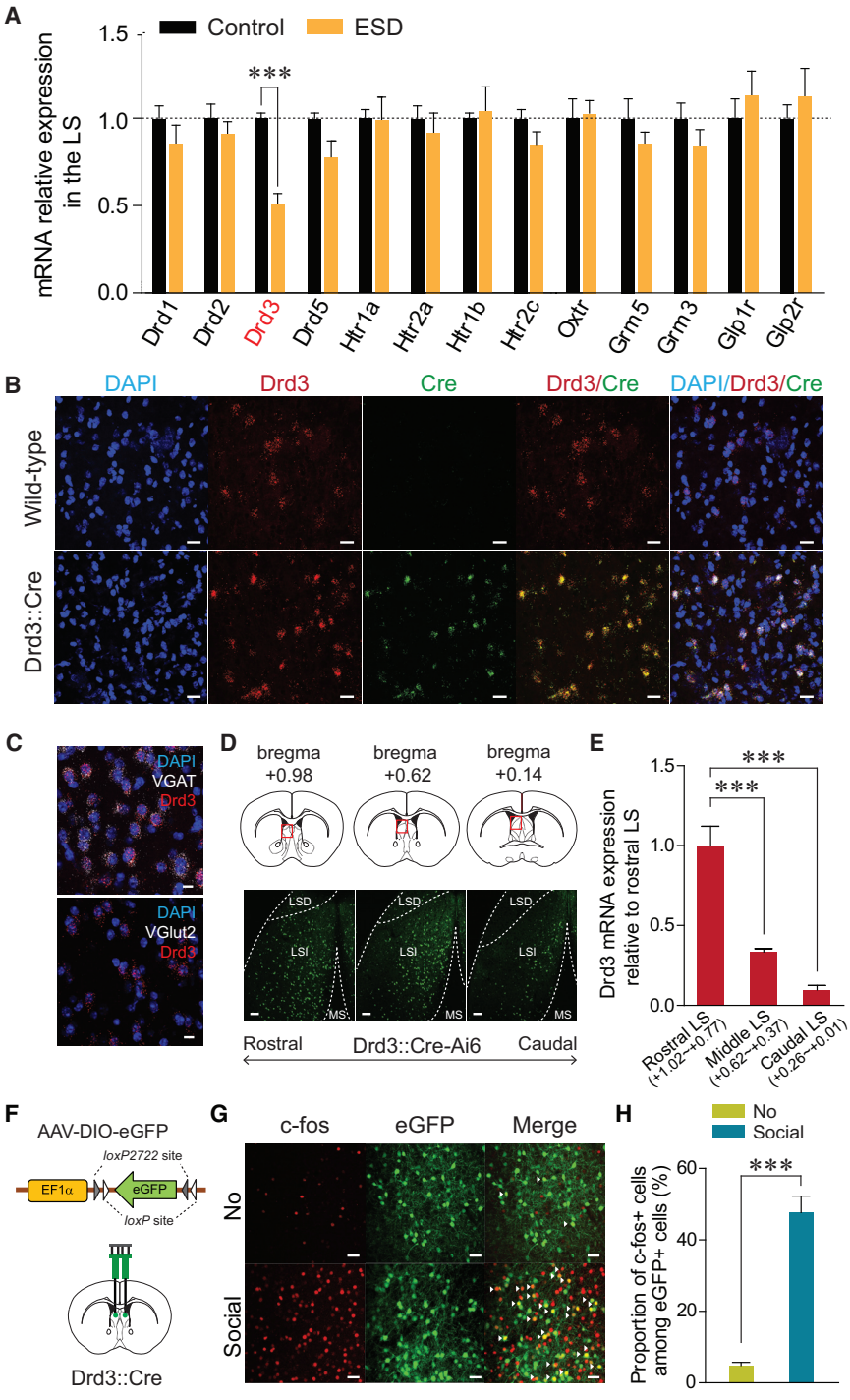

Figure 2. Reduced Drd3 mRNA in the LS of ESD Mice and Characterization of Drd3^{LS} Neurons

(A) Quantitative real-time PCR analysis of mRNA expression of several neuromodulator receptors in the LS. ESD mice showed significantly reduced Drd3 mRNA expression in the LS, but no changes in the other dopamine receptor subtypes (Drd1, Drd2, or Drd5), the serotonin receptors (Htr1a, Htr2a, Htr1b, Htr2c), an oxytocin receptor (Oxtr), metabotropic glutamate receptors (Grm3, Grm5), or glucagon receptors (Glp1r, Glp2r) (n = 5, 9 mice per group).

(B) Representative images of fluorescent *in situ* hybridizations of Drd3 mRNA (red) and Cre mRNA (green) expression in the LS of wild-type (top) or Drd3::Cre mice (bottom). Scale bars, 20 μm.

(C) Representative images of fluorescent *in situ* hybridizations of VGAT or VGlut2 mRNA (white) and Drd3 mRNA (red) in the LS of wild-type mice. Drd3 is expressed primarily in GABAergic neurons of the LS. Scale bars, 10 μm.

(D) Drd3 expression in the LS of Drd3::Cre-Ai6 mice. Coronal diagrams depicting the region analyzed (squared in red; top) and confocal images showing the Drd3 expression pattern in the LS along the rostral-caudal axis (bottom). Scale bars, 100 μm. LSD, lateral septal dorsal part; LSI, lateral septal intermediate part; MS, medial septum.

(E) The rostral, middle, and caudal LS was dissected at the indicated thickness, and Drd3 mRNA expression was measured by quantitative real-time PCR. Drd3 is expressed broadly across the LS, with the highest levels appearing in the rostral LS (n = 3 mice per group).

(F) Schematic for the bilateral injection of AAV expressing a Cre-dependent eGFP into the LS of control Drd3::Cre mice.

(G) Representative images showing c-*fos* immunoreactivity (red) and eGFP fluorescence (green) in the LS of control Drd3::Cre mice injected with AAV-DIO-eGFP following exposure to a social stimulus. White arrowheads indicate the co-localization of c-*fos* immunostaining with Drd3 expression. Scale bars, 40 μm.

(H) Quantification of the proportion of c-*fos*-positive cells among Drd3^{LS} neurons of control Drd3::Cre mice. Social stimuli elicited a robust increase of c-*fos* expression in Drd3^{LS} neurons (n = 4 mice per group).

Significance for multiple comparisons: unpaired t test (A and H), one-way ANOVA, post hoc, Fisher least significant difference (LSD) (E), **p < 0.01 ***p < 0.001. Data are presented as mean ± SEM. See also Figure S3.

(Figure S3Z) (Gunaydin et al., 2014; Hitti and Siegelbaum, 2014; Paredes, 2003; Wu et al., 2014).

Activity of Drd3^{LS} Neurons Is Blunted in ESD Mice in Response to Social Stimulus

Since Drd3 signaling has been suggested to modulate neuronal activity in several brain areas, it is possible that the endogenous activity of Drd3^{LS} neurons could encode key features of social behaviors (Chen et al., 2006; Gunaydin et al., 2014). We therefore asked how well Drd3^{LS} neuronal activity correlates with the incidence of social interaction behaviors. To do so, we injected the LS of control Drd3::Cre mice with AAV encoding a Ca^{2+} indicator (GCaMP6f) in a Cre-dependent manner and implanted an imaging cannula with a gradient index (GRIN) lens directly above the

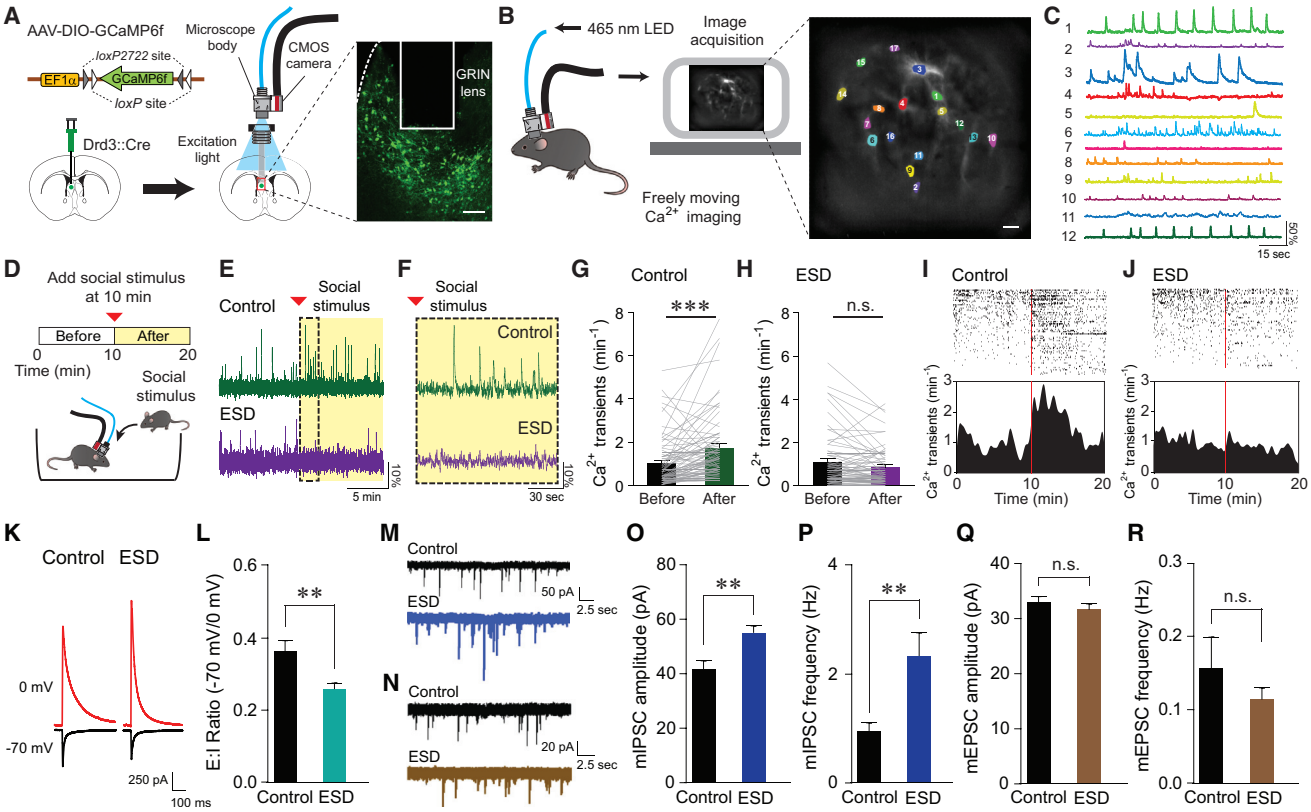

Figure 3. Drd3^{LS} Neurons of ESD Mice Display Reduced Activity in Response to Social Stimulus and Altered Synaptic Excitatory/Inhibitory Balance

(A) Schematic for the injection of AAV expressing GCaMP6f in a Cre-dependent manner into the LS of Drd3::Cre mice (left). Confocal image showing GRIN lens placement on the GCaMP6f-expressing Drd3^{LS} neurons. Scale bar, 200 μm (right).

(B) Illustration of *in vivo* Ca^{2+} imaging setup (left). Sample image of GCaMP6f-expressing Drd3^{LS} neurons and the color-coded regions of interest (ROIs) used for image analysis. Scale bar, 25 μm (right).

(C) Sample Ca^{2+} activity traces of $\Delta F/F_0$ from individual neurons in (B).

(D) Schematic for the experimental setup to record Ca^{2+} activity in GCaMP6f-expressing Drd3^{LS} neurons.

(E) Representative Ca^{2+} activity traces from Drd3^{LS} neurons of control (top, green) and ESD (bottom, purple) Drd3::Cre mice, with the yellow-shaded area indicating the presence of a social stimulus.

(F) Magnified view of the dotted box from (E).

(G and H) Average Ca^{2+} transients per minute in Drd3^{LS} neurons of control (G) and ESD (H) Drd3::Cre mice before and after the presentation of a social stimulus (n = 76 cells from 6 control mice, n = 66 cells from 5 ESD mice).

(I and J) Raster plots (top) and peristimulus time histograms (bottom) showing Drd3^{LS} neuronal activity of control (I) and ESD (J) Drd3::Cre mice (n = 76 cells from 6 control mice, n = 66 cells from 5 ESD mice). The rows and ticks in the raster plots represent individual cells and single Ca^{2+} transient events, respectively. Vertical red bars mark the time the social stimulus was introduced.

(K and L) Representative traces (K) and quantification (L) of synaptic E:I ratio recorded from Drd3^{LS} neurons of control and ESD Drd3::Cre mice (n = 19 cells from 3 control mice, n = 17 cells from 3 ESD mice).

(M and N) Representative traces of mIPSCs (M) and mEPSCs (N) from Drd3^{LS} neurons of control (top, black) and ESD Drd3::Cre mice (bottom, blue or brown).

(O and P) The Drd3^{LS} neurons of ESD Drd3::Cre mice showed enhanced mIPSC amplitude (O) and frequency (P) (n = 11 cells from 2 control mice, n = 13 cells from 3 ESD mice).

(Q and R) mEPSC amplitude (Q) and frequency (R) did not differ between control and ESD Drd3::Cre mice (n = 10 cells from 2 control mice, n = 14 cells from 3 ESD mice).

Significance for multiple comparisons: Paired t test (G), Mann-Whitney U test (L, O, and P), $^{**}p < 0.01$; $^{***}p < 0.001$; n.s., not significant. Data are presented as mean ± SEM.

See also Figure S4.

virus injection site (Figure 3A). Three weeks post-surgery, we imaged Ca^{2+} dynamics in Drd3^{LS} neurons with a mini-microscope and then quantified the number of *in vivo* Ca^{2+} transients per minute before and after introducing either a conspecific stranger (social stimulus) or a fake mouse (novel object) (Figures 3B, 3C, and S4A). Strikingly, we found significant increases in number of Ca^{2+} transients per minute in control Drd3::Cre mice during social interactions with the conspecific stranger (Figures S4B–S4D). In contrast, in the presence of a fake mouse, we did not observe any differences in Ca^{2+} transients of Drd3^{LS}

neurons even when control Drd3::Cre mice approached and investigated the fake mouse with physical contacts (Figures S4B–S4D). Notably, we found prominent increases in the average number of Ca^{2+} transients per minute under social contexts compared to novel object contexts (Figure S4D). This suggests that $Drd3^{LS}$ neuronal activity is more strongly correlated with actual social interactions than general novelty. Furthermore, we found that 64.7% of Ca^{2+} transients in $Drd3^{LS}$ neurons occurred at the onset of social bouts during male-male interactions (Figures S4E and S4F). Of those interactions, almost half (49.6%) of those Ca^{2+} transients were correlated with body-sniffing/mounting behaviors, while 33.3%, 17.1% of that occurred during following behaviors or nose to nose contacts, respectively (Figure S4G). We also observed that 56.5% of Ca^{2+} transients in $Drd3^{LS}$ neurons of control male mice interacting with a female mouse occurred at the onset of USVs (Figures S4H and S4I).

In light of our previous finding that ESD mice showed reduced expression of c-*fos* in the LS in response to social stimuli (Figures 1L and 1M), we hypothesized that the $Drd3^{LS}$ neuronal activity of ESD mice may show blunted responses to social stimuli. To examine this hypothesis, we compared average number of Ca^{2+} transients per minute in response to social stimuli between control and ESD mice. Consistent with our previous finding, we observed that social stimuli increased Ca^{2+} transients per minute in $Drd3^{LS}$ neurons of control Drd3::Cre mice. In contrast, the $Drd3^{LS}$ neurons of ESD Drd3::Cre mice exhibited no change in response to social stimuli (Figures 3D–3J and S4J). This suggests that $Drd3^{LS}$ neurons of ESD mice show impaired reactivity to social stimuli.

To uncover the synaptic mechanism by which $Drd3^{LS}$ neurons of ESD mice show blunted activity, we performed a whole-cell patch-clamp recording of $Drd3^{LS}$ neurons. We found a significant reduction in the ratio of evoked excitatory inputs to inhibitory inputs (E/I ratio) in ESD Drd3::Cre mice compared to controls (Figures 3K and 3L). This occurred without any accompanying change in the resting membrane potential, the rheobase, or in the ratio of the amplitudes of AMPA (a-amino-3-hydroxy-5-methyl-4-isoxazolepropionic acid) receptor-mediated excitatory postsynaptic currents (EPSCs) to NMDA (N-methyl-D-aspartate) receptor-mediated EPSCs (AMPAR/NMDAR ratio) (data not shown). Instead, we observed a significant increase in the amplitude and frequency of miniature inhibitory postsynaptic currents (mIPSCs) but not miniature EPSCs (mEPSCs) in the $Drd3^{LS}$ neurons of ESD Drd3::Cre mice (Figures 3M–3R). Together, these data suggest that $Drd3^{LS}$ neurons of ESD mice show blunted responses to social stimuli due to increased inhibitory synaptic inputs.

Bidirectional Modulation of $Drd3^{LS}$ Neuronal Activity Affects ESD-Induced Social Dysfunctions

Next, we asked whether the reduction of $Drd3^{LS}$ neuronal activity recapitulates the asocial behaviors of ESD mice. To determine this, we injected AAV expressing a Cre-dependent Kir2.1 potassium channel (AAV-DIO-GFP-Kir2.1), which reduces cellular activity by chronic hyperpolarization (Rothwell et al., 2014), into the LS of control Drd3::Cre mice (Figure 4A). Strikingly, we found that Kir2.1-induced silencing of $Drd3^{LS}$ neurons itself impairs both social preference and social communication with no accompanying change in locomotion or anxiety, mirroring the deficits of ESD mice (Figures 4B, 4D–4F, S5A, and S5B). However, similar silencing of Drd3-positive neurons in the NAc shell, another area that expresses high levels of Drd3 (Sokoloff et al., 1990), does not affect social preference, suggesting that the LS is a critical neural substrate where Drd3-expressing neurons regulate social behaviors (Figure 4C).

We next examined whether selective activation of $Drd3^{LS}$ neurons can reverse the social dysfunction of ESD mice. To achieve precise excitation of these cells with light, we expressed Channelrhodopsin2 (ChR2) in $Drd3^{LS}$ neurons of control Drd3::Cre or ESD Drd3::Cre mice, followed by the implantation of an optic cannula above the LS (Figure 4G). We subjected each mouse to the three-chamber test or the reciprocal social interaction test on two separate days with and without illumination (Figures 4H, S5C, and S5D). At baseline (light-off), consistent with our previous data, the ESD Drd3::Cre mice showed reduced social preference and fewer direct social contacts compared to control Drd3::Cre mice. In contrast, blue light-elicited activation of the $Drd3^{LS}$ neurons in ChR2-expressing ESD Drd3::Cre mice robustly reversed the impaired social interactions associated with early adversity (Figures 4I and S5E). In addition, ChR2-mediated stimulation of $Drd3^{LS}$ neurons rescued the USV defect of ESD Drd3::Cre mice, suggesting that the activation of $Drd3^{LS}$ neurons has a critical role in the protection against ESD-induced social impairment (Figures 4J, 4K, and S5F). Together, these results indicate that bi-directional modulation of $Drd3^{LS}$ neuronal activity can either aggravate or alleviate the social abnormalities induced by ESD.

Drd3 Agonist Treatment Enhances $Drd3^{LS}$ Neuronal Activity and Reverses ESD-Induced Social Impairments

Next, to examine whether Drd3 signaling plays a role in regulating the activity of the LS, we measured the expression of c-*fos* in the LS of both control and ESD mice 1 hr after intraperitoneal administration of the Drd3 agonist PD128907 (0.1 or 0.5 mg/kg i.p.). We found that PD128907 induced a robust and dose-dependent increase in c-*fos* immunoreactivity in the LS (Figures S5G and S5H). To further confirm the direct effect of PD128907 on LS neuronal activation, we performed an intracranial microinfusion of either saline or PD128907 (0.1 or 2.5 μg/side) into the LS. We observed that, in both control and ESD mice, local infusion of PD128907 also induced a remarkable increase of c-*fos* expression in rostral and middle part of the LS (bregma +0.98∼0.62) where most of the cannula tips were found (Figures 5A, 5B, and S5I). In contrast, regardless of drug treatment, we were not able to observe any changes of c-*fos* induction in caudal part of the LS (bregma +0.35∼+0.14) where we did not place any cannula tips (Figure S5J). Notably, we found that low dose of PD128907 (0.1 μg/side) induced less c-*fos* expression in the LS of ESD mice than control mice (Figure 5B). This suggests that the submaximal dose of PD128907 elicits a weaker response in the LS of ESD mice compared to controls, which consistent with our previous finding of reduced Drd3 signaling in the LS of ESD mice. Together, these findings demonstrate that pharmacological activation of Drd3 boosts neuronal activity in the LS.

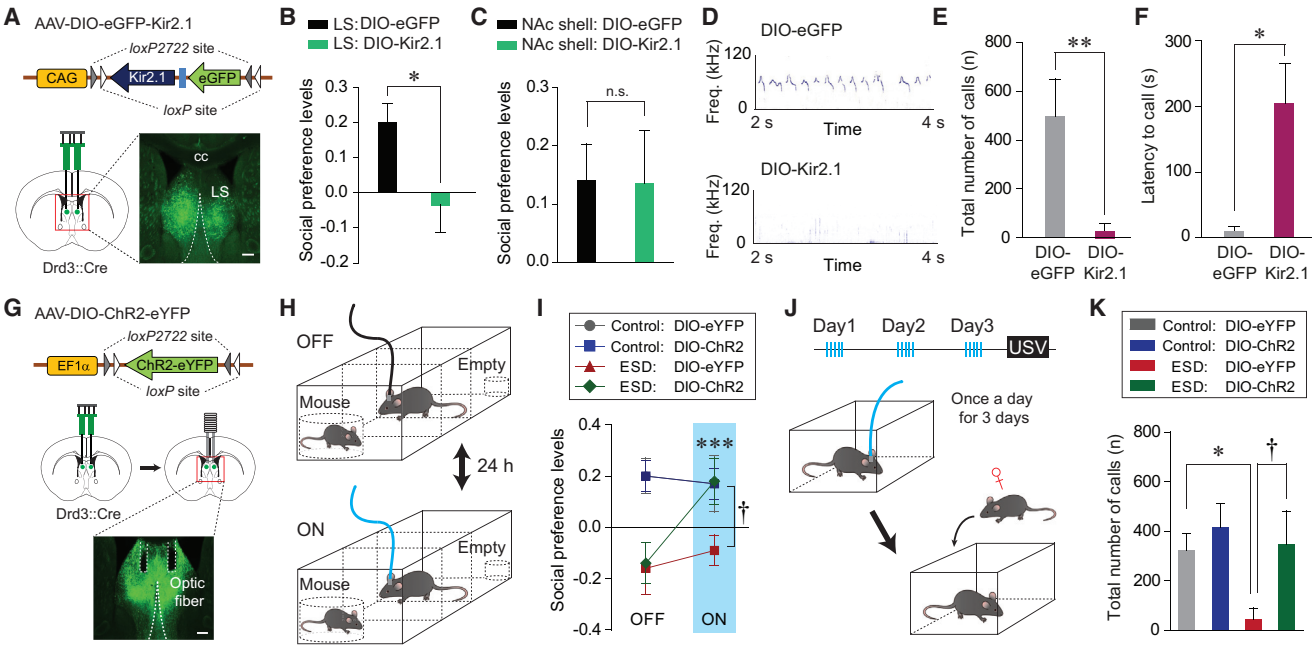

Figure 4. Modulation of Drd3^{LS} Neuronal Activity Influences Abnormal Social Behavior

(A) Schematic depicting the injection of AAV expressing a Cre-dependent Kir2.1 into the LS of Drd3::Cre mice. Scale bar, 250 μm. cc, corpus callosum.

(B and C) Social preference based on resident time in the three-chamber test. Viral-mediated Kir2.1 expression in Drd3^{LS} neurons reduced social preference (B, n = 8 mice per group), while similar silencing of Drd3$^{NAc\ shell}$ neurons did not affect social preference (C, n = 4 mice per group).

(D) Representative images of USVs emitted by control Drd3::Cre male mice injected with eGFP-expressing virus (top) or Kir2.1-expressing virus (bottom) in the LS, upon encountering a female mouse.

(E and F) Control Drd3::Cre mice expressing Kir2.1 in Drd3^{LS} neurons produced significantly fewer USVs (E) and showed increased latency to make the first USV call (F) (n = 6 mice per group).

(G) Schematic depicting the injection of AAV-DIO-ChR2-eYFP, followed by implantation of optic fibers above the virus injection site within the LS of Drd3::Cre mice (top and middle). Confocal image showing optic fiber placement in the LS (bottom). Scale bar, 250 μm.

(H) The experimental design of the three-chamber test with optical stimulation. Testing sessions were conducted twice and counterbalanced for order with a 24-hr interval between laser ON and laser OFF condition.

(I) Photostimulation of Drd3^{LS} neurons restored social preference in ESD Drd3::Cre mice (n = 6, 9 mice for each control group and n = 8, 11 mice for each ESD group; ***$p < 0.001$ compared with ESD mice expressing DIO-ChR2 during the OFF state; $^{\dagger}p < 0.05$ compared with ESD mice expressing DIO-eYFP during the ON state).

(J) The experimental design of the USV tests after repeated delivery of optical stimulation (once a day for 3 days) (top). After the last stimulation, a female mouse was placed for recording USVs produced by male mice (bottom).

(K) Photoactivation of Drd3^{LS} neurons rescued the number of USVs emitted by ESD Drd3::Cre mice to the levels of controls (n = 7, 8 mice for each control group and n = 7, 6 mice for each ESD group).

Significance for multiple comparisons: unpaired t test (B), Mann-Whitney U test (E and F), two-way repeated-measures (RM) ANOVA; post hoc, Fisher LSD (I), and two-way ANOVA; post hoc, Bonferroni (K), *$p < 0.05$; **$p < 0.01$; ***$p < 0.001$; $^{\dagger}p < 0.05$; n.s., not significant. Data are presented as mean ± SEM.

See also Figure S5.

Consistent with previous reports (Chen et al., 2006; Diaz et al., 2011; Swant et al., 2008), we found that bath application of PD128907 to brain slices of control Drd3::Cre mice significantly reduced the mean amplitude of the evoked IPSCs in Drd3^{LS} neurons (Figures 5C and 5D). We also confirmed via *in vivo* Ca^{2+} imaging that PD128907 injection (0.5 mg/kg, i.p.) induced a substantial increase in the average number of Ca^{2+} transients per minute in Drd3^{LS} neurons of control Drd3::Cre mice, and that this increase then slowly returned to baseline (Figures 5E–5H). These data suggest that the activation of Drd3 signaling via the Drd3 agonist PD128907 enhances the activity of Drd3^{LS} neurons by suppressing their inhibitory synaptic inputs.

This led us to hypothesize that the activation of Drd3^{LS} neuronal signaling may be able to rescue the social dysfunction of ESD mice by upregulating Drd3^{LS} neuronal activity. To test this, we microinjected either saline or PD128907 directly into the LS of control or ESD mice and found that PD128907 produced a dose-dependent improvement in the social preference of ESD mice (Figures 6A–6C and S6A). Moreover, we further confirmed that systemic injection of PD128907 (0.5 mg/kg, i.p.) normalized ESD-induced abnormal social behaviors both in the three-chamber test and the USV test (Figures 6D–6F, S6B, and S6C). In contrast, chronic injections of fluoxetine (20 mg/kg, i.p.), a commonly prescribed antidepressant to treat psychiatric diseases with accompanying social dysfunctions (Van Amerigen et al., 1993; Hollander et al., 2012), did not ameliorate the impaired social preference of ESD mice (Figures 6D, 6E, and S6B). This suggests that mice exposed to early adversity may

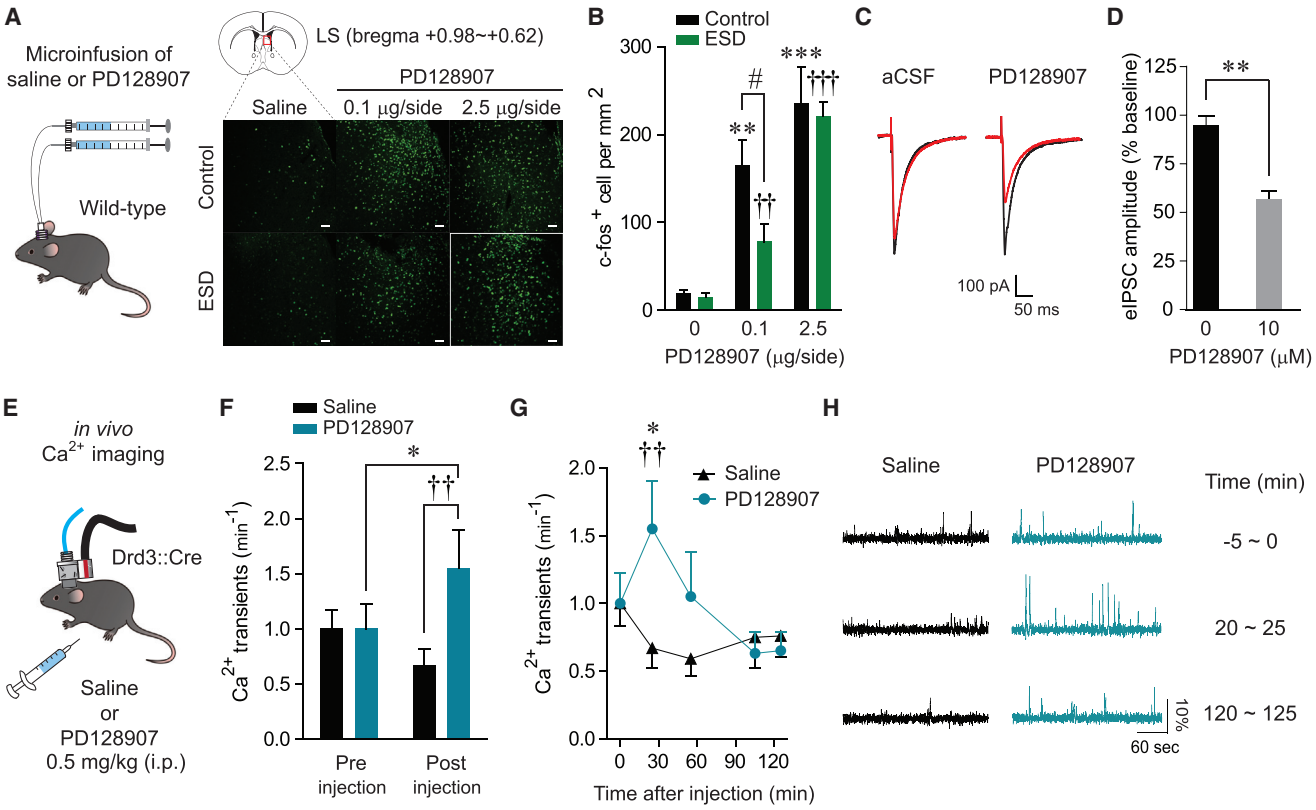

Figure 5. Administration of the Drd3 Agonist PD128907 Increases Drd3^{LS} Neuronal Activity

(A) Schematic for the microinjection of saline or PD128907 into the LS of control and ESD mice (left). Representative images of c-*fos* staining in the LS of control and ESD mice following microinfusion of saline or PD128907 (0.1 or 2.5 μg/side). Scale bars, 50 μm (right).

(B) Quantification of c-*fos*-positive cells in the LS of control or ESD mice 1 hr after saline or PD128907 microinfusion. PD128907 activated the LS neurons both in control and ESD mice (n = 6, 6, and 8 mice for each control group and n = 6, 8, and 6 mice for each ESD group; $^{**}p < 0.01$, $^{***}p < 0.001$ compared with control mice infused with saline; $^{††}p < 0.01$, $^{†††}p < 0.001$ compared with ESD mice infused with saline; $^{\#}p < 0.05$ compared with ESD mice infused with 0.1 μg/side of PD128907).

(C) Representative traces of electrically evoked IPSCs (eIPSCs) recorded from Drd3^{LS} neurons of control Drd3::Cre mice prior to (black) and after (red) bath application of artificial cerebrospinal fluid (aCSF) or PD128907 (10 μM).

(D) The amplitude of eIPSCs showed a significant reduction following a 20-min exposure to 10 μM PD128907 (n = 5, 7 cells per group).

(E) Schematic for recording the activity from GCaMP6f-expressing Drd3^{LS} neurons of control Drd3::Cre mice treated with saline or PD128907 (0.5 mg/kg, i.p.).

(F) Average Ca^{2+} transients per minute before and 20 min after saline or PD128907 injections (n = 28 cells from 3 mice treated with saline, n = 21 cells from 3 mice treated with PD129907).

(G) Time course of changes in Ca^{2+} transients per minute was measured during a 5-min window of pre-injection (at −5 min) and post-injection (at 20, 50, 100, 120 min). PD128907 administration induced a significant increase in GCaMP6f activity of Drd3^{LS} neurons, which then gradually returned to baseline levels (n = 28 cells from 3 mice treated with saline, n = 21 cells from 3 mice treated with PD129907; $^{*}p < 0.05$ compared with PD128907-treated mice before injection; $^{††}p < 0.01$ compared with saline-treated mice at 20 min after injection).

(H) Representative Ca^{2+} activity traces from Drd3^{LS} neurons of control Drd3::Cre mice at each 5-min window of pre-injection and post-injection.

Significance for multiple comparisons: two-way ANOVA; post hoc, Bonferroni (B), Mann-Whitney U test (D), and two-way RM ANOVA; post hoc, Fisher LSD (F and G), $^{\#}p < 0.05$; $^{*}p < 0.05$; $^{**}p < 0.01$; $^{††}p < 0.01$. Data are presented as mean ± SEM.

See also Figure S5.

have a distinct biological endophenotype that leads to differing responses to conventional treatments.

To further investigate an extended role for Drd3 in protecting against social defects, we asked whether PD128907 can correct the aberrant social phenotypes of the inbred mouse strain BTBR T+tf/J (BTBR), which is a preclinical model of autism (McFarlane et al., 2008). Remarkably, PD128907 treatment (0.5 mg/kg, i.p.) rescued the impaired social preference of BTBR mice, suggesting that PD128907 may also have an efficacy against for heritable forms of autistic social dysfunction (Figures S6D and S6E). Surprisingly, we also found that BTBR mice showed significantly reduced expression of Drd3 mRNA in the LS compared with age-matched C57/BL6 mice. In addition, this change was not accompanied by alterations in other subtypes of dopamine receptor such as Drd1 and Drd2 (Figures S6F and S6G), indicating a similar molecular defect as the one we observed in ESD mice. This suggests that downregulation of Drd3 signaling in the LS may be the important molecular change leading to impaired social preference in BTBR mice as well as the social dysfunctions of mice exposed to early adversity.

Since systemic treatments generally affect the whole brain, we next asked whether the LS is specifically required for this rescue

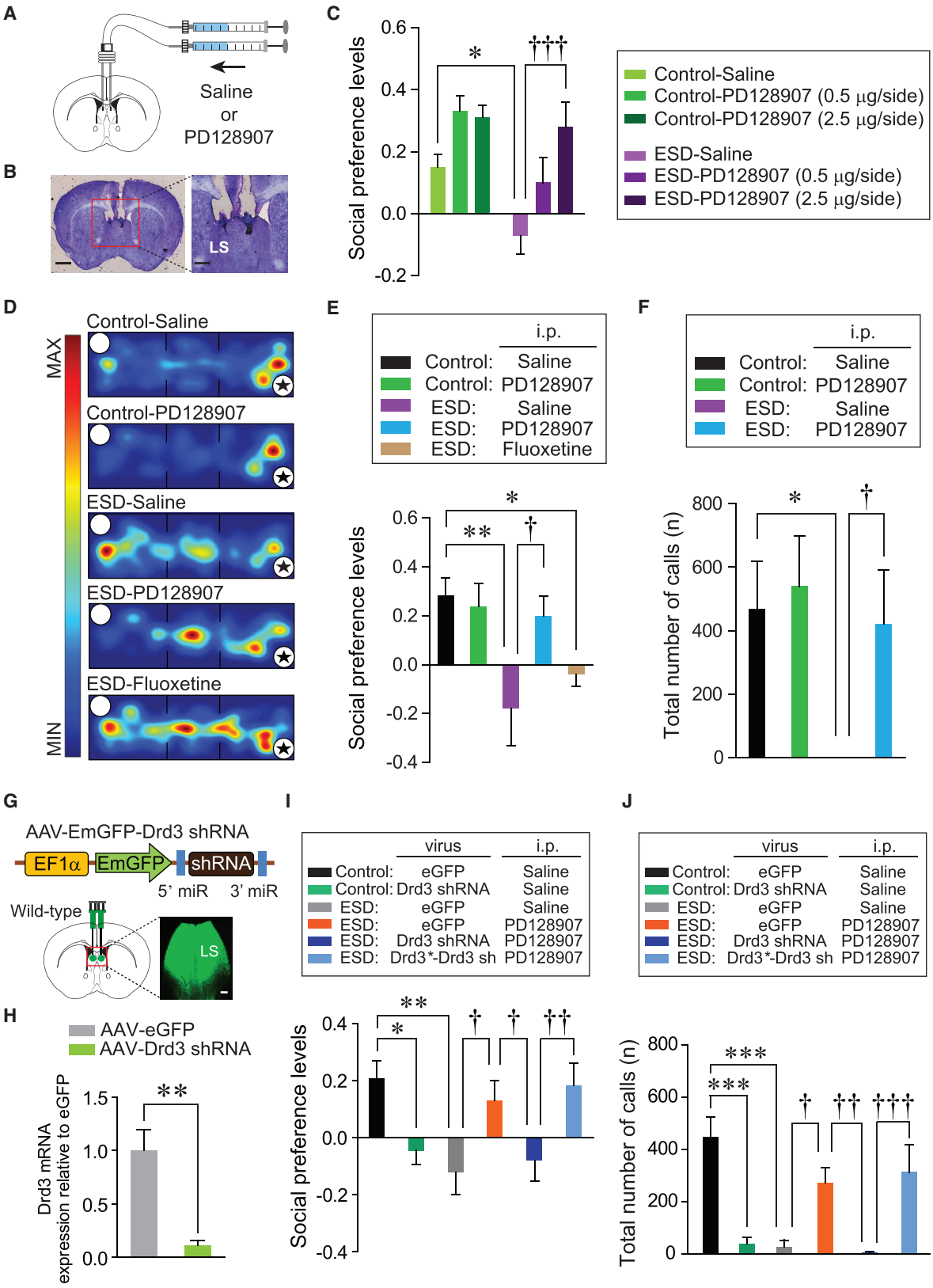

(legend on next page)

of ESD-induced social dysfunction by intraperitoneal injection of PD128907. To this end, we took advantage of AAV expressing short hairpin RNA (shRNA) against Drd3 (AAV-Drd3 shRNA), which robustly reduced endogenous Drd3 mRNA levels in the LS (Figures 6G and 6H). After delivering these viruses to the LS of control mice, we found that the resulting knockdown of Drd3 signaling in the LS recapitulated the social impairments (e.g., impaired social preference and communication deficits) of ESD mice (Figures 6I, 6J, S7A, and S7B). A similar knockdown of Drd3 signaling in the LS of ESD mice prevented PD128907 treatment from rescuing their social defects, while ESD mice injected with a control virus (AAV-eGFP) still showed PD128907-induced behavioral normalization (Figures 6I, 6J, S7A, and S7B). To rule out potential off-target effects of shRNA manipulation, we expressed a shRNA-resistant Drd3 (Drd3*) along with the shRNA against Drd3 (AAV-Drd3*-Drd3 sh) in the LS. We found that co-expression of Drd3* prevented the Drd3 knockdown from inhibiting the PD128907-induced behavioral rescue of the social defects in ESD mice (Figures 6I, 6J, S7A, and S7B). This confirms that effects of shRNA against Drd3 are indeed mediated by knockdown of Drd3 signaling. Finally, to further confirm the specificity of the Drd3 shRNA, we asked whether $Drd3^{LS}$ neuron-specific expression of Drd3* can reverse the effect of Drd3 knockdown in the LS of ESD Drd3::Cre mice (Figures S7C and S7D). Consistent with our previous results, the specific knockdown of Drd3 signaling in the LS of ESD Drd3::Cre mice (AAV-DIO-Drd3 shRNA) blocked the PD128907-induced rescue of the social preference defect in ESD mice. However, we did not observe this blockade in ESD Drd3::Cre mice that expressed both Drd3* and shRNA against Drd3 (AAV-DIO Drd3*-Drd3 sh) in the LS (Figure S7E) after PD128907 treatment (0.5 mg/kg, i.p.). This confirms again that shRNA manipulation exerted its effects without any unexpected off-target effects. Together, these data strongly support that the activation of Drd3 signaling in the LS is required for PD128907-induced improvement of the social defects in ESD mice.

DISCUSSION

Exposure to family adversity or social deprivation during childhood is linked to social anxiety, impaired social skills, and poor communication in adulthood. As such, it can be acknowledged to be a predictor of adult antisocial behaviors (Bruce et al., 2012; Dodge et al., 1990; Enoch et al., 2010). Likewise, postnatal stress is also detrimental in rodents. This is particularly true in the critical period of early infancy while the offspring are entirely dependent on their mother for survival. Several ''maternal separation'' (MS) paradigms in which periodic disruption of social bonding by separating pups from their mother have been devised to study the impact of early life factors on adult life (Huot et al., 2002; Uchida et al., 2010). Here, we adopted a slightly modified version of the maternal separation procedure: the ''ESD'' paradigm (McCormick et al., 1998; Zimmerberg et al., 2009). Unlike the more common maternal separation paradigms, which keep littermates together, the ESD paradigm subject pups to complete social isolation by physically excluding them from their dams and littermates. Moreover, we employed an unpredictable stress schedule by randomizing the timing of the deprivation period, making it more difficult to anticipate. Given that unpredictable stress has more profound and persistent effects than predictable stress (Enthoven et al., 2008), we believe that our ESD model would better replicate the etiological factors implicated in psychiatric disorders by including this uncertainty. Indeed, we found that our approach with this ESD model allowed us to investigate aberrant social behaviors in adult life, including reduced social preference levels, impaired social interactions, and severe social communication deficits, all of which are core symptoms of psychiatric diseases such as ASD and MDD (Figure 1).

Numerous studies have strongly suggested a functional role for Drd3 in the social disruptions associated with psychiatric disorders such as ASD (de Krom et al., 2009; Staal et al., 2015). For example, polymorphisms in Drd3 are associated with repetitive and stereotyped behaviors in ASD (Staal et al., 2012). Drd3

Figure 6. Pharmacological Activation of Drd3 Signaling in the LS Prevents Social Impairments of ESD Mice

(A) Schematic for the microinjection of saline or PD128907 into the LS of control and ESD mice.

(B) Image shows the location of the cannula tips in the LS. Scale bars, 1 mm (left) and 250 μm (right).

(C) Microinjection of PD128907 into the LS produced a dose-dependent increase in the social preference of ESD mice in the three-chamber test (n = 5, 5, and 4 mice for each control group; n = 9, 5, and 6 mice for each ESD group).

(D) Representative heatmap images during three-chamber tests for control or ESD mice treated with saline, PD128907 (0.5 mg/kg, i.p.), or fluoxetine (20 mg/kg, i.p.). Asterisks indicate the presence of a conspecific stranger.

(E) Social preference levels based on resident time in the three-chamber test. PD128907 (0.5 mg/kg, i.p.) administration increased social preference in ESD mice to the level of control mice, whereas chronic injection of fluoxetine (20 mg/kg, i.p.) did not (n = 6, 5 mice for each control group, n = 6, 6, and 5 mice for each ESD group).

(F) PD128907 (0.5 mg/kg, i.p.) administration restored the total number of USVs in ESD mice (n = 5, 6 mice for each control group, n = 6, 6 mice for each ESD group).

(G) Schematic depicting the injection of AAV expressing Drd3 shRNA into the LS of wild-type mice. Scale bar, 250 μm.

(H) Quantitative real-time PCR analysis of Drd3 mRNA expression from the LS of mice injected with eGFP- or Drd3 shRNA-expressing AAV (n = 4 mice per group).

(I and J) Knockdown of Drd3 by injection of AAV-Drd3 shRNA into the LS attenuated social preference (I) and total number of USVs (J) in control mice and blocked the PD128907-induced rescue of impaired social preference (I) and communication deficits (J) in ESD mice. However, the expression of shRNA-resistant Drd3 (Drd3*, the mutant form is indicated by an asterisk) together with the shRNA against Drd3 (AAV-Drd3*-Drd3 sh) did not block the PD128907-induced rescue of the social dysfunctions in ESD mice. (I, n = 11, 10 mice for each control group, n = 9, 10, 11, and 11 mice for each ESD group). (J, n = 8, 10 mice for each control group, n = 7, 8, 9, and 10 mice for each ESD group).

Significance for multiple comparisons: two-way ANOVA; post hoc, Bonferroni (C and F), one-way ANOVA; post hoc, Fisher LSD (E, I, and J), and unpaired t test (H), *$p < 0.05$; **$p < 0.01$; ***$p < 0.001$; $^{\dagger}p < 0.05$; $^{\dagger\dagger}p < 0.01$; $^{\dagger\dagger\dagger}p < 0.001$. Data are presented as mean ± SEM.

See also Figures S6 and S7.

expression is limited mainly to parts of the limbic system that are involved in motivated behavior (Murray et al., 1994; Sokoloff et al., 1990). In the LS, Drd3 is expressed predominantly in the rostromedial part (Figure 2), a subregion that receives the majority of the LS-projecting dopaminergic terminals from the VTA (Reddy et al., 2016). Interestingly, we found significant increases in c-*fos* expression in the VTA as well as the LS of control mice in response to social stimuli (Figure S2). This is consistent with previous studies that suggested that the activity dynamics of the VTA projections encode key features of social interactions and that dopaminergic signaling in its downstream structures is involved in social reward and social behaviors (Gunaydin et al., 2014).

We found that $Drd3^{LS}$ neurons have dense reciprocal connections with the MPA and AHA (Figure S3). This is an important observation for three reasons. First, given that the LS receives GABAergic inputs from the hypothalamus (Dietrich and Horvath, 2009; Gallagher et al., 1995), we speculate that the MPA or AHA can be the major sources of these inhibitory inputs onto $Drd3^{LS}$ neurons. It is, therefore, plausible that the MPA or AHA GABAergic inputs to $Drd3^{LS}$ neurons of ESD mice may be increased in number or may display increased release probability, thereby contributing to ESD-induced downregulation of $Drd3^{LS}$ neuronal activity. Second, because both the AHA and MPA are essential nodes for various social behaviors (Ferris et al., 1997; McHenry et al., 2017), engaging LS-MPA and/or LS-AHA circuit activity may override predisposition to social dysfunction induced by early adversity. Moreover, the AHA is a major integrator of neural processes related to aggression and defense during social interactions with same-sex conspecifics (Ferris et al., 1997; Goodson et al., 2012), while the MPA is more likely to be involved in sexual behaviors and encode attractive social cues from opposite-sex conspecifics (McHenry et al., 2017; Paredes et al., 1990). This raises the possibility that the $Drd3^{LS}$ neurons modulate the various aspects of ESD-induced social dysfunction in a projection-specific manner (e.g., reduced social preference during male-male interaction versus communication deficits during male-female interaction). Third, previous studies have shown that AHA-projecting LS neurons regulate the function of the hypothalamus-pituitary-adrenal (HPA) axis as well as corticosterone levels via presumptive di-synaptic disinhibitory connections with the paraventricular nucleus (PVN) (Anthony et al., 2014; Herman et al., 2002). In addition, many clinical and preclinical reports have suggested that early adversity is characterized by lifelong disruptions of the homeostatic mechanisms that regulate the HPA axis (Enthoven et al., 2008; Lyons et al., 1998; Pfeffer et al., 2007). Thus, ESD may exert at least some of its effects by altering the activity of AHA-projecting $Drd3^{LS}$ neurons, which would then contribute to the dysregulation of the HPA axis. Future studies focusing further on $Drd3^{LS}$ neuronal circuitry will expand our understanding of how the cell-type-specific and/or projection-specific neural circuits of the LS interact to precipitate social impairments after early adverse experiences.

Clinical studies showed that the psychiatric symptoms of patients with a history of adverse early life experiences respond more poorly to pharmacotherapy than those of similar patients without such a history (Bruce et al., 2012; Nanni et al., 2012; Nemeroff, 2016). This implies that ELS exerts long-term physiological consequences linked to an individual's unique endophenotype and that patients with ELS may require alternative treatment options. Interestingly, we observed that, although the commonly prescribed antidepressant fluoxetine had no effect on the social impairments of ESD mice, treatment with the PD128907 rescued their severe social defects (Figure 6). This suggests that manipulation of Drd3 signaling may be an alternative therapeutic strategy for treating the social dysfunction induced or exacerbated by early adversity.

The BTBR mouse is an inbred strain that displays the core symptoms of autism (McFarlane et al., 2008). Although previous studies of BTBR mice have addressed the anatomical features of their brains and changes in neurotransmitter levels (Squillace et al., 2014; Stephenson et al., 2011), little is known about the specific neural substrates or the neuromodulatory signaling whose own modulation affects social dysfunction of BTBR mice. Consistent with previous reports (Stephenson et al., 2011), we found that the LS of BTBR mice showed significant lateral displacement (Figure S6F), implicating that BTBR mice may have altered anatomical LS circuitry. We also found that BTBR mice exhibited downregulation of Drd3 signaling in the LS and that the administration of PD128907 rescues their social impairments (Figure S6). Although further studies are needed, these data support a broad role for $Drd3^{LS}$ neuronal signaling in the pathophysiology of social dysfunctions that are associated with environmental stressors as well as with genetic factors.

It is important to note that the activation of Drd3 signaling in the LS modulates synaptic transmission and neuronal activity. We observed that PD128907 inhibits evoked IPSCs and increases the activity of $Drd3^{LS}$ neurons of control mice (Figure 5). Although the mechanisms that couple Drd3 to intracellular signal transduction systems are not yet well defined *in vivo*, previous studies have suggested that Drd3 activation increases neuronal activity by inhibiting PKA. This, in turn, would increase the endocytosis of $GABA_A$ receptors (Chen et al., 2006; Swant et al., 2008). Furthermore, recent studies have suggested that Drd3's effects on neuronal activity may depend on the regional localization of Drd3 in glutamatergic versus GABAergic neurons (Li and Kuzhikandathil, 2012). For example, excitatory glutamatergic neurons are likely inhibited by Drd3 activation, whereas GABAergic neurons are activated by Drd3 activation because Drd3 suppresses GABA-receptor-mediated inhibitory synaptic transmission by increasing $GABA_A$ receptor endocytosis (Chen et al., 2006; Swant et al., 2008). Given that LS neurons are predominantly GABAergic (Figure 2), we speculate that activation of Drd3 signaling in the LS may modulate $GABA_A$ receptor trafficking and enhance the LS neuronal activity by reducing GABAergic transmission.

In summary, we have uncovered a novel mechanism underlying early life stress-induced adult social dysfunction. Our findings reveal a role for the $Drd3^{LS}$ neuronal signaling and its corresponding neuronal activity in mediating ELS-induced social dysfunctions. This is a significant advance in our understanding of the neural mechanisms by which adverse events early in life can alter the activity of specific neural circuits and cause behavioral dysfunction in adulthoods. Our results may provide promising information for the development of novel therapeutic strategies

that target adverse childhood experience-related symptomatology associated with numerous neuropsychiatric illnesses.

STAR★METHODS

Detailed methods are provided in the online version of this paper and include the following:

- KEY RESOURCES TABLE
- CONTACT FOR REAGENT AND RESOURCE SHARING
- EXPERIMENTAL MODEL AND SUBJECT DETAILS
- METHOD DETAILS
  - ESD Procedures
  - Behavioral Assays
  - Immunohistochemistry for c-*fos*
  - Brain Dissection and Quantitative Real-Time PCR
  - Fluorescent *In Situ* Hybridization (FISH)
  - Virus and shRNA Generation
  - Stereotaxic Surgeries
  - Optogenetic Stimulation
  - *In Vivo* Ca^{2+} Imaging in Freely Moving Mice and Data Analysis
  - Slice Electrophysiology Recordings
  - Drugs
  - Intracranial Drug Injection and Histology
- QUANTIFICATION AND STATISTICAL ANALYSIS

SUPPLEMENTAL INFORMATION

Supplemental Information includes six figures and can be found with this article online at https://doi.org/10.1016/j.neuron.2017.11.040.

ACKNOWLEDGMENTS

We acknowledge Dr. X. Wang for providing MATLAB code for analyzing behavioral data and *in vivo* Ca^{2+} imaging data. We also thank M.N. Askar and J. Chang for technical assistance with analyzing behavioral data, Dr. A. Pinto-Duarte for his scientific input, and K. Kim for her help with illustrations. This study was supported by the Klingenstein foundation, Searle scholar program (15-SSP-229; Kinship foundation), Whitehall foundation (2014-08-63), NARSAD young investigator award (24094), and a grant from NIMH (R01MH107742). S. Shin is supported by a Tobacco-related disease research program (TRDRP, 25FT-0007) postdoctoral fellowship. H. Pribiag is supported by a Canadian Institutes of Health Research (CHIR) Fellowship. V. Lilascharoen is supported by the Anandamahidol Foundation Fellowship.

AUTHOR CONTRIBUTIONS

S.S. and B.K.L. designed the study and interpreted the results. S.S. performed all the experiments and analyzed the data. H.P. performed and analyzed all the electrophysiological experiments. S.S. and V.L. designed and generated the viruses. D.K. helped with the FISH experiments. X.-Y.W. helped with virus production. S.S. and B.K.L wrote the manuscript with contributions from all authors.

DECLARATION OF INTERESTS

The authors declare no competing interests.

Received: June 6, 2017
Revised: October 17, 2017
Accepted: November 29, 2017
Published: December 21, 2017

REFERENCES

Agid, O., Shapira, B., Zislin, J., Ritsner, M., Hanin, B., Murad, H., Troudart, T., Bloch, M., Heresco-Levy, U., and Lerer, B. (1999). Environment and vulnerability to major psychiatric illness: A case control study of early parental loss in major depression, bipolar disorder and schizophrenia. Mol. Psychiatry *4*, 163–172.

Anthony, T.E., Dee, N., Bernard, A., Lerchner, W., Heintz, N., and Anderson, D.J. (2014). Control of stress-induced persistent anxiety by an extra-amygdala septohypothalamic circuit. Cell *156*, 522–536.

Bambini-Junior, V., Zanatta, G., Della Flora Nunes, G., Mueller de Melo, G., Michels, M., Fontes-Dutra, M., Nogueira Freire, V., Riesgo, R., and Gottfried, C. (2014). Resveratrol prevents social deficits in animal model of autism induced by valproic acid. Neurosci. Lett. *583*, 176–181.

Bandelow, B., Charimo Torrente, A., Wedekind, D., Broocks, A., Hajak, G., and Rüther, E. (2004). Early traumatic life events, parental rearing styles, family history of mental disorders, and birth risk factors in patients with social anxiety disorder. Eur. Arch. Psychiatry Clin. Neurosci. *254*, 397–405.

Bolger, K.E., and Patterson, C.J. (2001). Developmental pathways from child maltreatment to peer rejection. Child Dev. *72*, 549–568.

Bruce, L.C., Heimberg, R.G., Blanco, C., Schneier, F.R., and Liebowitz, M.R. (2012). Childhood maltreatment and social anxiety disorder: Implications for symptom severity and response to pharmacotherapy. Depress. Anxiety *29*, 131–138.

Calipari, E.S., Bagot, R.C., Purushothaman, I., Davidson, T.J., Yorgason, J.T., Peña, C.J., Walker, D.M., Pirpinias, S.T., Guise, K.G., Ramakrishnan, C., et al. (2016). In vivo imaging identifies temporal signature of D1 and D2 medium spiny neurons in cocaine reward. Proc. Natl. Acad. Sci. USA *113*, 2726–2731.

Callaway, E.M., and Luo, L. (2015). Monosynaptic circuit tracing with glycoprotein-deleted rabies viruses. J. Neurosci. *35*, 8979–8985.

Chen, G., Kittler, J.T., Moss, S.J., and Yan, Z. (2006). Dopamine D3 receptors regulate GABAA receptor function through a phospho-dependent endocytosis mechanism in nucleus accumbens. J. Neurosci. *26*, 2513–2521.

Chung, W., Choi, S.Y., Lee, E., Park, H., Kang, J., Park, H., Choi, Y., Lee, D., Park, S.-G., Kim, R., et al. (2015). Social deficits in IRSp53 mutant mice improved by NMDAR and mGluR5 suppression. Nat. Neurosci. *18*, 435–443.

de Krom, M., Staal, W.G., Ophoff, R.A., Hendriks, J., Buitelaar, J., Franke, B., de Jonge, M.V., Bolton, P., Collier, D., Curran, S., et al. (2009). A common variant in DRD3 receptor is associated with autism spectrum disorder. Biol. Psychiatry *65*, 625–630.

Diaz, M.R., Chappell, A.M., Christian, D.T., Anderson, N.J., and McCool, B.A. (2011). Dopamine D3-like receptors modulate anxiety-like behavior and regulate GABAergic transmission in the rat lateral/basolateral amygdala. Neuropsychopharmacology *36*, 1090–1103.

Dietrich, M.O., and Horvath, T.L. (2009). GABA keeps up an appetite for life. Cell *137*, 1177–1179.

Dodge, K.A., Bates, J.E., and Pettit, G.S. (1990). Mechanisms in the cycle of violence. Science *250*, 1678–1683.

Enoch, M.A., Steer, C.D., Newman, T.K., Gibson, N., and Goldman, D. (2010). Early life stress, MAOA, and gene-environment interactions predict behavioral disinhibition in children. Genes Brain Behav. *9*, 65–74.

Enthoven, L., Oitzl, M.S., Koning, N., van der Mark, M., and de Kloet, E.R. (2008). Hypothalamic-pituitary-adrenal axis activity of newborn mice rapidly desensitizes to repeated maternal absence but becomes highly responsive to novelty. Endocrinology *149*, 6366–6377.

Felix-Ortiz, A.C., and Tye, K.M. (2014). Amygdala inputs to the ventral hippocampus bidirectionally modulate social behavior. J. Neurosci. *34*, 586–595.

Ferris, C.F., Melloni, R.H., Jr., Koppel, G., Perry, K.W., Fuller, R.W., and Delville, Y. (1997). Vasopressin/serotonin interactions in the anterior hypothalamus control aggressive behavior in golden hamsters. J. Neurosci. *17*, 4331–4340.

Fischer, J., and Hammerschmidt, K. (2011). Ultrasonic vocalizations in mouse models for speech and socio-cognitive disorders: Insights into the evolution of vocal communication. Genes Brain Behav. *10*, 17–27.

Gallagher, J.P., Zheng, F., Hasuo, H., and Shinnick-Gallagher, P. (1995). Activities of neurons within the rat dorsolateral septal nucleus (DLSN). Prog. Neurobiol. *45*, 373–395.

Goff, B., Gee, D.G., Telzer, E.H., Humphreys, K.L., Gabard-Durnam, L., Flannery, J., and Tottenham, N. (2013). Reduced nucleus accumbens reactivity and adolescent depression following early-life stress. Neuroscience *249*, 129–138.

Goodson, J.L., Kelly, A.M., Kingsbury, M.A., and Thompson, R.R. (2012). An aggression-specific cell type in the anterior hypothalamus of finches. Proc. Natl. Acad. Sci. USA *109*, 13847–13852.

Gunaydin, L.A., Grosenick, L., Finkelstein, J.C., Kauvar, I.V., Fenno, L.E., Adhikari, A., Lammel, S., Mirzabekov, J.J., Airan, R.D., Zalocusky, K.A., et al. (2014). Natural neural projection dynamics underlying social behavior. Cell *157*, 1535–1551.

Guzmán, Y.F., Tronson, N.C., Jovasevic, V., Sato, K., Guedea, A.L., Mizukami, H., Nishimori, K., and Radulovic, J. (2013). Fear-enhancing effects of septal oxytocin receptors. Nat. Neurosci. *16*, 1185–1187.

Han, S., Tai, C., Westenbroek, R.E., Yu, F.H., Cheah, C.S., Potter, G.B., Rubenstein, J.L., Scheuer, T., de la Iglesia, H.O., and Catterall, W.A. (2012). Autistic-like behaviour in Scn1a+/- mice and rescue by enhanced GABA-mediated neurotransmission. Nature *489*, 385–390.

Hanson, J.L., Albert, D., Iselin, A.M.R., Carré, J.M., Dodge, K.A., and Hariri, A.R. (2016). Cumulative stress in childhood is associated with blunted reward-related brain activity in adulthood. Soc. Cogn. Affect. Neurosci. *11*, 405–412.

Harasta, A.E., Power, J.M., von Jonquieres, G., Karl, T., Drucker, D.J., Housley, G.D., Schneider, M., and Klugmann, M. (2015). Septal glucagon-like peptide 1 receptor expression determines suppression of cocaine-induced behavior. Neuropsychopharmacology *40*, 1969–1978.

Heath, R.G. (1963). Electrical self-stimulation of the brain in man. Am. J. Psychiatry *120*, 571–577.

Heim, C., and Nemeroff, C.B. (2001). The role of childhood trauma in the neurobiology of mood and anxiety disorders: preclinical and clinical studies. Biol. Psychiatry *49*, 1023–1039.

Herman, J.P., Cullinan, W.E., Ziegler, D.R., and Tasker, J.G. (2002). Role of the paraventricular nucleus microenvironment in stress integration. Eur. J. Neurosci. *16*, 381–385.

Hitti, F.L., and Siegelbaum, S.A. (2014). The hippocampal CA2 region is essential for social memory. Nature *508*, 88–92.

Hollander, E., Soorya, L., Chaplin, W., Anagnostou, E., Taylor, B.P., Ferretti, C.J., Wasserman, S., Swanson, E., and Settipani, C. (2012). A double-blind placebo-controlled trial of fluoxetine for repetitive behaviors and global severity in adult autism spectrum disorders. Am. J. Psychiatry *169*, 292–299.

Huot, R.L., Plotsky, P.M., Lenox, R.H., and McNamara, R.K. (2002). Neonatal maternal separation reduces hippocampal mossy fiber density in adult Long Evans rats. Brain Res. *950*, 52–63.

Jamain, S., Radyushkin, K., Hammerschmidt, K., Granon, S., Boretius, S., Varoqueaux, F., Ramanantsoa, N., Gallego, J., Ronnenberg, A., Winter, D., et al. (2008). Reduced social interaction and ultrasonic communication in a mouse model of monogenic heritable autism. Proc. Natl. Acad. Sci. USA *105*, 1710–1715.

Kendler, K.S., Karkowski, L.M., and Prescott, C.A. (1999). Causal relationship between stressful life events and the onset of major depression. Am. J. Psychiatry *156*, 837–841.

Kessler, R.C., Davis, C.G., and Kendler, K.S. (1997). Childhood adversity and adult psychiatric disorder in the US National Comorbidity Survey. Psychol. Med. *27*, 1101–1119.

Kohls, G., Schulte-Rüther, M., Nehrkorn, B., Müller, K., Fink, G.R., Kamp-Becker, I., Herpertz-Dahlmann, B., Schultz, R.T., and Konrad, K. (2013). Reward system dysfunction in autism spectrum disorders. Soc. Cogn. Affect. Neurosci. *8*, 565–572.

Lee, J., Chung, C., Ha, S., Lee, D., Kim, D.-Y., Kim, H., and Kim, E. (2015). Shank3-mutant mice lacking exon 9 show altered excitation/inhibition balance, enhanced rearing, and spatial memory deficit. Front. Cell. Neurosci. *9*, 94.

Li, Y., and Kuzhikandathil, E.V. (2012). Molecular characterization of individual D3 dopamine receptor-expressing cells isolated from multiple brain regions of a novel mouse model. Brain Struct. Funct. *217*, 809–833.

Luo, A.H., Tahsili-Fahadan, P., Wise, R.A., Lupica, C.R., and Aston-Jones, G. (2011). Linking context with reward: A functional circuit from hippocampal CA3 to ventral tegmental area. Science *333*, 353–357.

Lyons, D.M., Kim, S., Schatzberg, A.F., and Levine, S. (1998). Postnatal foraging demands alter adrenocortical activity and psychosocial development. Dev. Psychobiol. *32*, 285–291.

Ma, H.T., On, K.F., Tsang, Y.H., and Poon, R.Y.C. (2007). An inducible system for expression and validation of the specificity of short hairpin RNA in mammalian cells. Nucleic Acids Res. *35*, e22.

McCormick, C.M., Kehoe, P., and Kovacs, S. (1998). Corticosterone release in response to repeated, short episodes of neonatal isolation: Evidence of sensitization. Int. J. Dev. Neurosci. *16*, 175–185.

McFarlane, H.G., Kusek, G.K., Yang, M., Phoenix, J.L., Bolivar, V.J., and Crawley, J.N. (2008). Autism-like behavioral phenotypes in BTBR T+tf/J mice. Genes Brain Behav. *7*, 152–163.

McHenry, J.A., Otis, J.M., Rossi, M.A., Robinson, J.E., Kosyk, O., Miller, N.W., McElligott, Z.A., Budygin, E.A., Rubinow, D.R., and Stuber, G.D. (2017). Hormonal gain control of a medial preoptic area social reward circuit. Nat. Neurosci. *20*, 449–458.

Mesic, I., Guzman, Y.F., Guedea, A.L., Jovasevic, V., Corcoran, K.A., Leaderbrand, K., Nishimori, K., Contractor, A., and Radulovic, J. (2015). Double dissociation of the roles of metabotropic glutamate receptor 5 and oxytocin receptor in discrete social behaviors. Neuropsychopharmacology *40*, 2337–2346.

Moretti, P., Bouwknecht, J.A., Teague, R., Paylor, R., and Zoghbi, H.Y. (2005). Abnormalities of social interactions and home-cage behavior in a mouse model of Rett syndrome. Hum. Mol. Genet. *14*, 205–220.

Murgatroyd, C., Patchev, A.V., Wu, Y., Micale, V., Bockmühl, Y., Fischer, D., Holsboer, F., Wotjak, C.T., Almeida, O.F., and Spengler, D. (2009). Dynamic DNA methylation programs persistent adverse effects of early-life stress. Nat. Neurosci. *12*, 1559–1566.

Murray, A.M., Ryoo, H.L., Gurevich, E., and Joyce, J.N. (1994). Localization of dopamine D3 receptors to mesolimbic and D2 receptors to mesostriatal regions of human forebrain. Proc. Natl. Acad. Sci. USA *91*, 11271–11275.

Nanni, V., Uher, R., and Danese, A. (2012). Childhood maltreatment predicts unfavorable course of illness and treatment outcome in depression: A meta-analysis. Am. J. Psychiatry *169*, 141–151.

Nemeroff, C.B. (2016). Paradise lost: the neurobiological and clinical consequences of child abuse and neglect. Neuron *89*, 892–909.

Olds, J., and Milner, P. (1954). Positive reinforcement produced by electrical stimulation of septal area and other regions of rat brain. J. Comp. Physiol. Psychol. *47*, 419–427.

Osakada, F., and Callaway, E.M. (2013). Design and generation of recombinant rabies virus vectors. Nat. Protoc. *8*, 1583–1601.

Paredes, R.G. (2003). Medial preoptic area/anterior hypothalamus and sexual motivation. Scand. J. Psychol. *44*, 203–212.

Paredes, R., Haller, A.E., Manero, M.C., Alvarado, R., and Ågmo, A. (1990). Medial preoptic area kindling induces sexual behavior in sexually inactive male rats. Brain Res. *515*, 20–26.

Paxinos, G., and Franklin, K.B.J. (2008). The Mouse Brain in Stereotaxic Coordinates, Third Edition (Academic Press), pp. 1–350.

Pfeffer, C.R., Altemus, M., Heo, M., and Jiang, H. (2007). Salivary cortisol and psychopathology in children bereaved by the september 11, 2001 terror attacks. Biol. Psychiatry *61*, 957–965.

Rai, D., Golding, J., Magnusson, C., Steer, C., Lewis, G., and Dalman, C. (2012). Prenatal and early life exposure to stressful life events and risk of autism spectrum disorders: Population-based studies in Sweden and England. PLoS ONE *7*, e38893.

Reddy, I.A., Pino, J.A., Weikop, P., Osses, N., Sørensen, G., Bering, T., Valle, C., Bluett, R.J., Erreger, K., Wortwein, G., et al. (2016). Glucagon-like peptide 1 receptor activation regulates cocaine actions and dopamine homeostasis in the lateral septum by decreasing arachidonic acid levels. Transl. Psychiatry *6*, e809.

Risold, P.Y., and Swanson, L.W. (1997). Chemoarchitecture of the rat lateral septal nucleus. Brain Res. Brain Res. Rev. *24*, 91–113.

Rothwell, P.E., Fuccillo, M.V., Maxeiner, S., Hayton, S.J., Gokce, O., Lim, B.K., Fowler, S.C., Malenka, R.C., and Südhof, T.C. (2014). Autism-associated neuroligin-3 mutations commonly impair striatal circuits to boost repetitive behaviors. Cell *158*, 198–212.

Schmittgen, T.D., and Livak, K.J. (2008). Analyzing real-time PCR data by the comparative C(T) method. Nat. Protoc. *3*, 1101–1108.

Sheehan, T.P., Chambers, R.A., and Russell, D.S. (2004). Regulation of affect by the lateral septum: Implications for neuropsychiatry. Brain Res. Brain Res. Rev. *46*, 71–117.

Silverman, J.L., Yang, M., Lord, C., and Crawley, J.N. (2010). Behavioural phenotyping assays for mouse models of autism. Nat. Rev. Neurosci. *11*, 490–502.

Singewald, G.M., Rjabokon, A., Singewald, N., and Ebner, K. (2011). The modulatory role of the lateral septum on neuroendocrine and behavioral stress responses. Neuropsychopharmacology *36*, 793–804.

Sokoloff, P., Giros, B., Martres, M.P., Bouthenet, M.L., and Schwartz, J.C. (1990). Molecular cloning and characterization of a novel dopamine receptor (D3) as a target for neuroleptics. Nature *347*, 146–151.

Squillace, M., Dodero, L., Federici, M., Migliarini, S., Errico, F., Napolitano, F., Krashia, P., Di Maio, A., Galbusera, A., Bifone, A., et al. (2014). Dysfunctional dopaminergic neurotransmission in asocial BTBR mice. Transl. Psychiatry *4*, e427.

Staal, W.G., de Krom, M., and de Jonge, M.V. (2012). Brief report: the dopamine-3-receptor gene (DRD3) is associated with specific repetitive behavior in autism spectrum disorder (ASD). J. Autism Dev. Disord. *42*, 885–888.

Staal, W.G., Langen, M., van Dijk, S., Mensen, V.T., and Durston, S. (2015). DRD3 gene and striatum in autism spectrum disorder. Br. J. Psychiatry *206*, 431–432.

Stephenson, D.T., O'Neill, S.M., Narayan, S., Tiwari, A., Arnold, E., Samaroo, H.D., Du, F., Ring, R.H., Campbell, B., Pletcher, M., et al. (2011). Histopathologic characterization of the BTBR mouse model of autistic-like behavior reveals selective changes in neurodevelopmental proteins and adult hippocampal neurogenesis. Mol. Autism *2*, 7.

Swant, J., Stramiello, M., and Wagner, J.J. (2008). Postsynaptic dopamine D3 receptor modulation of evoked IPSCs via GABA(A) receptor endocytosis in rat hippocampus. Hippocampus *18*, 492–502.

Tejeda, H.A., Wu, J., Kornspun, A.R., Lowell, B.B., Carlezon, W.A., Tejeda, H.A., Wu, J., et al. (2017). Pathway- and cell-specific kappa-opiod receptor modulation of excitation-inhibition balance differentially gates D1 and D2 accumbens neuron activity. Neuron *93*, 147–163.

Tsai, P.T., Hull, C., Chu, Y., Greene-Colozzi, E., Sadowski, A.R., Leech, J.M., Steinberg, J., Crawley, J.N., Regehr, W.G., and Sahin, M. (2012). Autistic-like behaviour and cerebellar dysfunction in Purkinje cell Tsc1 mutant mice. Nature *488*, 647–651.

Uchida, S., Hara, K., Kobayashi, A., Funato, H., Hobara, T., Otsuki, K., Yamagata, H., McEwen, B.S., and Watanabe, Y. (2010). Early life stress enhances behavioral vulnerability to stress through the activation of REST4-mediated gene transcription in the medial prefrontal cortex of rodents. J. Neurosci. *30*, 15007–15018.

Van Ameringen, M., Mancini, C., and Streiner, D.L. (1993). Fluoxetine efficacy in social phobia. J. Clin. Psychiatry *54*, 27–32.

Wu, Z., Autry, A.E., Bergan, J.F., Watabe-Uchida, M., and Dulac, C.G. (2014). Galanin neurons in the medial preoptic area govern parental behaviour. Nature *509*, 325–330.

Zhao, C., Eisinger, B., and Gammie, S.C. (2013). Characterization of GABAergic neurons in the mouse lateral septum: A double fluorescence in situ hybridization and immunohistochemical study using tyramide signal amplification. PLoS ONE *8*, e73750.

Zimmerberg, B., Foote, H.E., and Van Kempen, T.A. (2009). Olfactory association learning and brain-derived neurotrophic factor in an animal model of early deprivation. Dev. Psychobiol. *51*, 333–344.

STAR★METHODS

KEY RESOURCES TABLE

REAGENT or RESOURCE	SOURCE	IDENTIFIER
Antibodies		
Rabbit monoclonal anti-c-Fos (9F6)	Cell Signaling Technology	Cat# 2250S; RRID: AB_2247211
Goat anti-Rabbit IgG (H+L) Highly Cross-Adsorbed Secondary Antibody, Alexa Fluor Plus 488	Thermo Fisher Scientific	Cat# A32731; RRID: AB_2633280
Goat anti-Rabbit IgG (H+L) Highly Cross-Adsorbed Secondary Antibody, Alexa Fluor Plus 555	Thermo Fisher Scientific	Cat# A32732; RRID: AB_2633281
Bacterial and Virus Strains		
EnvA-pseudotyped glycoprotein (G)-deleted rabies virus expressing eGFP (EnvA-RVΔG-eGFP)	Lim Lab	N/A
Chemicals, Peptides, and Recombinant Proteins		
(+)-PD 128907 hydrochloride	Tocris	Cat# 1243
Fluoxetine hydrochloride	Sigma-Aldrich	Cat# F132
NBQX	Tocris	Cat# 0373
Picrotoxin	Sigma	Cat# P1675
Critical Commercial Assays		
Drd3	Advanced Cell Diagnostics	Cat# 447721
Cre	Advanced Cell Diagnostics	Cat# 312281
Slc32a1 (VGAT)	Advanced Cell Diagnostics	Cat# 319191
Slc17a6 (VGlut2)	Advanced Cell Diagnostics	Cat# 319171
Hybrid-R RNA purification kit	GeneAll Biotechnology	Cat# 305-101
Experimental Models: Organisms/Strains		
Mouse: Drd3::Cre: B6.FVB(Cg)-Tg(Drd3-cre) KI196Gsat/Mmucd	GENSAT	Stock# 036968-UCD; RRID: MMRRC_036968-UCD
Mouse: Ai6: B6.Cg-Gt(ROSA)26Sor$^{tm6(CAG-ZsGreen1)Hze}$/J	The Jackson Laboratory	JAX: 007906; RRID: IMSR_JAX:007906
Mouse: C57BL/6J	The Jackson Laboratory	JAX: 000664; RRID: IMSR_JAX:000664
Mouse: BTBR: BTBR T+ Itpr3tf/J	The Jackson Laboratory	JAX: 002282; RRID: IMSR_JAX:002282
Oligonucleotides		
shRNA targeting sequence: Drd3: 5′-TTCTTCTT GACTCACGTTCTT-3′	This paper	N/A
Primers for mouse Drd3 (F:5′- ATGGCACCTCT GAGCCAGATAAG-3′; R: 5′-TCAGCAGGAT AGAATCTTGAGGAAGG-3′)	This paper	N/A
Drd3 (Mm00432887_m1)	Life Technologies	Cat# 4331182
Drd1 (Mm02620146_s1)	Life Technologies	Cat# 4331182
Drd2 (Mm00438545_m1)	Life Technologies	Cat# 4331182
Drd5 (Mm04210376_s1)	Life Technologies	Cat# 4331182
Htr1a (Mm00434106_s1)	Life Technologies	Cat# 4331182
Htr2a (Mm00555764_m1)	Life Technologies	Cat# 4331182
Htr1b (Mm00439377_s1)	Life Technologies	Cat# 4331182
Htr2c (Mm00434127_m1)	Life Technologies	Cat# 4331182
Oxtr (Mm01329577_g1)	Life Technologies	Cat# 4331182
Grm3 (Mm00725298_m1)	Life Technologies	Cat# 4331182
Grm5 (Mm00690332_m1)	Life Technologies	Cat# 4331182
Glp1r (Mm00445292_m1)	Life Technologies	Cat# 4331182
Glp2r (Mm01329475_m1)	Life Technologies	Cat# 4331182
GAPDH (Mm99999915_g1)	Life Technologies	Cat# 4331182

(*Continued on next page*)

Continued

REAGENT or RESOURCE	SOURCE	IDENTIFIER
Recombinant DNA		
AAV_{DJ}-EF1α-eGFP	This paper	N/A
AAV_{DJ}-EF1α-DIO-eGFP	This paper	N/A
AAV_{DJ}-hSyn-DIO-mRuby2-P2A-TVA-RVG	This paper	N/A
AAV_{DJ}-EF1α-DIO-GCaMP6f	This paper	N/A
AAV_{DJ}-CAG-DIO-eGFP-P2A-Kir2.1	This paper	N/A
AAV_{DJ}- EF1α-DIO-eYFP	This paper	N/A
AAV_{DJ}-EF1α-DIO-hChR2(H134R)-eYFP	Plasmid: Karl Deisseroth Production: Lim Lab	Addgene #55639
AAV_{DJ}- EF1α-EmGFP-Drd3 shRNA	This paper	N/A
AAV_{DJ}- EF1α-Drd3*-P2A-EmGFP-Drd3 shRNA	This paper	N/A
AAV_{DJ}- EF1α-DIO-EmGFP-Drd3 shRNA	This paper	N/A
AAV_{DJ}- EF1α-DIO-Drd3*-P2A-EmGFP-Drd3 shRNA	This paper	N/A
Software and Algorithms		
QuantStudio Real-Time PCR Software	Applied Biosystems	N/A
UltraVox XT (v.3.0)	Noldus	http://www.noldus.com/animal-behavior-research/products/ultravox-xt
MATLAB R2015a	MathWorks	N/A
Doric Neuroscience Studio software (v.4.0.1)	Doric Lenses	http://doriclenses.com/life-sciences/software/955-doric-neuroscience-studio.html
FIJI (ImageJ)	NIH	https://fiji.sc/
Viewer II	BIOBSERVE	http://www.biobserve.com/behavioralresearch/products/viewer
SigmaStat (v.3.5)	Aspire Software	N/A
Other		
Dual fiber-optic cannula	Doric Lenses	DFC_200/240-0.22_10 mm_GS0.6_FLT
Complementary metal-oxide-semiconductor (CMOS) camera	Doric Lenses	SFMB_L_UFGJ_1000_458
Snap-in imaging cannula model L	Doric Lenses	SICL_V_500_5.66_120
Guide cannula	Plastics One	C235GS-5-0.6/SPC
Dummy cannula	Plastics One	C235DCS-5/SPC
Internal cannula	Plastics One	C235IS-5/SPC

CONTACT FOR REAGENT AND RESOURCE SHARING

Further information and requests for resources and reagents should be directed to and will be fulfilled by the Lead Contact, Byung Kook Lim (bklim@ucsd.edu).

EXPERIMENTAL MODEL AND SUBJECT DETAILS

C57BL/6J and BTBR T+ Itpr3tf/J mice were obtained from the Jackson Laboratory. Drd3::Cre bacterial artificial chromosome (BAC) transgenic mice were from the Gene Expression Nervous System Atlas (GENSAT, Founder line: KI196) and were crossed for several generations to C57BL/6J mice before using. To visualize Drd3-positive neurons, Drd3::Cre mice were crossed with Ai6 mice (ZsGreen1 reporter line; Jackson Laboratory). Adult male mice (8-12 weeks old) were used for behavioral experiments, immunohistochemistry, and slice electrophysiology. Both male and female mice (8-12 weeks old) were used for quantitative real-time PCR, FISH, and anatomical tracing. Mice were housed on a 12-h light/dark cycle with rodent chow and water *ad libitum*. All behavioral procedures were performed during the light cycle. Prior to testing, mice were acclimated to the test room for at least 1 h. All experiments were approved by the Institutional Animal Care and Use Committee (IACUC) of the University of California, San Diego.

METHOD DETAILS

ESD Procedures

The ESD stress paradigm was adopted from previously published methods with minor modifications (Murgatroyd et al., 2009; Uchida et al., 2010; Zimmerberg et al., 2009). Briefly, pregnant female mice were individually housed when they were 14-16 d pregnant. From postnatal day 1 (P1) to P14, ESD pups were separated from both their dam and littermates for 3 h each day. During this separation, ESD pups were placed individually in a divided small chamber with clean bedding and transferred to an incubator which was maintained at 32 ± 1°C. The timing of the separation period was randomized, but within the light cycle (9:00 a.m. to 4:00 p.m.). At the end of the separation period, ESD pups were reunited with the dam and littermates. Control pups remained undisturbed in the maternal nest. All pups were weaned at P21 and housed in groups of three to five of the same gender until the start of the experiments.

Behavioral Assays

Locomotion

Locomotion was assessed in an open field arena (44 × 44 × 44 cm^3). Mice were placed individually to the arena and allowed to explore freely for 15-30 min. Activity was monitored using a webcam mounted above the arena and analyzed by tracking software (BIOBSERVE). For the time course data analysis, the distance traveled was measured in 5-min bins.

Open Field Test

Each individual mouse was placed in the open field arena (44 × 44 × 44 cm^3) and allowed to move freely for 15 min. The open field area was subdivided into two zones, a center (20 × 20 cm^2) and periphery. The movement of mice was monitored with a webcam and analyzed by tracking software (BIOBSERVE).

Elevated Plus Maze

The elevated plus maze consisted of two open arms, two closed arms, and a center, elevated to a height of 30.5 cm above the ground. Mice were placed in the center and allowed to explore the space for 5 min. The movement of mice was analyzed by tracking software (BIOBSERVE).

Novel Object Recognition Test

Mice were habituated to the open field arena (44 × 44 × 44 cm^3) in the absence of objects for 30 min a day before the training session. During the training session, two identical objects were placed in each corner of the arena, and mice were allowed to explore for 10 min. Twenty-four hours after training, mice were placed in the arena where one of the two objects was replaced with a novel object having different color and shape. All movements of mice were monitored with a webcam for 10 min, and the recognition time in each object area (2 cm around the object) was measured by tracking software (BIOBSERVE). Discrimination rate was calculated as [(time spent in a novel object area) / (time spent in a novel object area + time spent in a familiar object area) × 100 (%)] (Lee et al., 2015).

Buried Food Olfactory Test

This experiment was performed as previously described (Chung et al., 2015). Briefly, mice were given strawberry chocolate cookies and water *ad libitum* for 2 d before testing. Mice were deprived of cookies for 12 h before testing. During testing, a small piece of cookie was buried at the corner of the cage under 2 cm of bedding. The subject mouse was introduced at the opposite end of the cookie burial site. The time for the mouse to find the buried cookie and begin to burrow was measured. Fresh cages and bedding were used for every test.

Three-Chamber Social Preference Test

The test was performed as described previously, with minor modifications (Han et al., 2012). A non-transparent plexiglass box (68 × 22 × 24 cm^3) with two partitions that make two side chambers (left and right; 28 × 22 × 24 cm^3) separated by a central chamber (12 × 22 × 24 cm^3) was used. In the first 10-min session, the test mouse was placed in the middle of the three-chamber apparatus and allowed to habituate to the apparatus where two empty wire cages were located in the left and right chambers. In the second 10-min session, an age and gender-matched stranger mouse was placed in one of the wire cages on the side designated as the 'social' compartment, whereas the other side contained an empty wire cage. The designation of the 'social' side was randomly assigned in a counterbalanced fashion. The movement of the mouse was monitored by a webcam and was analyzed by tracking software (BIOBSERVE). The amount of time mice spent in each compartment (resident time), and the amount of time mice explored within a 2 cm radius proximal to each wire cage (sniffing time) were measured. Social preference levels were calculated as [(time in the social compartment - time in the empty compartment) / (time in social compartment + time in the empty compartment)] (Bambini-Junior et al., 2014).

Reciprocal Social Interaction Test

As a stranger animal, male juvenile mice (4-5 weeks old) were used instead of adults to avoid mutual aggression (Moretti et al., 2005). Each testing mouse spent 30 min in an open field arena (44 × 44 × 44 cm^3) for a habituation. After that, a stranger mouse was introduced to the arena and allowed to explore freely for 5 min. All behaviors were video recorded and analyzed by two experimenters blind to the testing conditions and then the data were averaged. Reciprocal social interactions were defined as activities including close following (< 1 cm), body sniffing, mounting, and nose to nose contact.

USV Test

USVs were examined as described previously (Chung et al., 2015; Fischer and Hammerschmidt, 2011). For habituations, male mice were individually placed inside of a soundproof recording chamber for 30 min. Subsequently, one estrus female was placed in the

recording chamber, and the male mouse was allowed to investigate the female for 5 min, during which emitted USVs were recorded using UltraVox XT software (version 3.0; Noldus) (Tsai et al., 2012).

Immunohistochemistry for c-*fos*

For quantification of c-*fos* immunoreactivity after social contacts, mice were individually housed on the day before testing day. On the testing day, a stranger male juvenile mouse (social stimulus) was introduced in the cage and allowed to interact with the experimental mouse for 10 min. The experimental mice were transcardially perfused with 4% PFA 30 min after introducing the social stimulus. Brains were extracted and post-fixed overnight in 4% PFA. Coronal sections (50 μm) were immunostained using a rabbit anti-c-*fos* antibody (1:5000; Cell Signaling Technology) applied overnight in a PBS solution containing 0.3% Triton X-100 (PBS-T), at room temperature. Sections were then washed in PBS-T and incubated in a 1:500 dilution of goat anti-rabbit IgG (H+L) highly cross-adsorbed secondary antibodies, Alexa Fluor Plus 488 or 555 (Thermo Fisher Scientific) in PBS-T for 1 h. The sections were rinsed with PBS-T and mounted using mounting medium. Images were acquired using a confocal microscope (Olympus FluoView FV1200) and quantitatively analyzed with ImageJ.

Brain Dissection and Quantitative Real-Time PCR

Mice were anesthetized with isofluorane and 250 μm slices were prepared in oxygenated aCSF, using a vibratome (Leica VT1200). The LS was microdissected bilaterally, and samples were immediately frozen on dry ice and stored at −80°C prior to RNA isolation. Total RNA was extracted from dissected samples using Hybrid-R RNA purification kit (GeneAll Biotechnology). Purified RNA samples were reverse transcribed by using the SuperScript-III First-strand cDNA synthesis kit (Invitrogen). Quantitative real-time PCR was performed by using TaqMan Gene Expression Assay Kit (Applied Biosystems). All TaqMan probes were purchased from Applied Biosystems and are as follows: Drd3 (Mm00432887_m1), Drd1 (Mm02620146_s1), Drd2 (Mm00438545_m1), Drd5 (Mm04210376_s1), Htr1a (Mm00434106_s1), Htr2a (Mm00555764_m1), Htr1b (Mm00439377_s1), Htr2c (Mm00434127_m1), Oxtr (Mm01329577_g1), Grm3 (Mm00725298_m1), Grm5 (Mm00690332_m1), Glp1r (Mm00445292_m1), Glp2r (Mm01329475_m1) and glyceraldhyde-3-phosphate dehydrogenase (GAPDH; Mm99999915_g1). Target amplification was performed by using ViiA 7 Real-Time PCR System (Applied Biosystems). The relative mRNA expression levels were calculated via a comparative threshold cycle (C_t) method using GAPDH as an internal control: $\Delta C_t = C_t$ (gene of interest) – C_t (GAPDH). The gene expression fold change was normalized to the control sample and then was calculated as $2^{-\Delta\Delta Ct}$ (Schmittgen and Livak, 2008).

Fluorescent *In Situ* Hybridization (FISH)

Brains were rapidly extracted and flash frozen with isopentane (Sigma-Aldrich) chilled with dry ice in 70% ethanol. Coronal brain slices (20 μm) containing the LS were sectioned on a cryostat (Leica CM3050S) at −20°C. Brain slices were mounted directly onto slides and stored at −80°C until FISH processing. The FISH was conducted using RNAscope probes (Advanced Cell Diagnostics, ACD) (Tejeda et al., 2017). Slides were fixed in 4% PFA for 15 min at 4°C and subsequently dehydrated for 5-10 min with 50%, 70% and 100% ethanol at room temperature. Sections were then incubated with a Protease pretreat-IV solution for 30 min, and washed with PBS, before being incubated with probes for 2 h at 40°C in the HybEZ oven (ACD). All probes used were commercially available: Mm-Drd3-C1 (NM 007877.1), Cre recombinase-C2 (KC 845567.1), Mm-Slc17a7(VGlut2)-C2 (NM 182993.2) and Mm-Slc32a1(VGAT)-C3 (NM 009508.2). After washing with wash buffer, the signal was amplified by incubating tissue sections in amplification buffers at 40°C. After the final rinse, DAPI solution was applied to the sections. Slides were coverslipped and visualized with a confocal microscope (Olympus FluoView FV1200).

Virus and shRNA Generation

AAV was produced by transfection of 293 cells with three plasmids: an AAV vector expressing target constructs (eGFP, DIO-eGFP, DIO-mRuby2-TVA-RVG, DIO-GCaMP6f, DIO-eGFP-Kir2.1, DIO-ChR2(H134R)-eYFP, DIO-eYFP, EmGFP-Drd3 shRNA, Drd3*-EmGFP-Drd3 shRNA, DIO-EmGFP-Drd3 shRNA, DIO-Drd3*-EmGFP-Drd3 shRNA), AAV helper plasmid (pHELPER; Agilent) and AAV rep-cap helper plasmid (pRC-DJ, gift from M. Kay). At 72 h after transfection, the cells were collected and lysed. Viral particles were then purified by an iodixanol step-gradient ultracentrifugation method. The iodixanol was diluted and the AAV was concentrated using a 100-kDa molecular mass cutoff ultrafiltration device. The genomic titer was determined by quantitative real-time PCR. The AAV vectors were diluted in PBS to a working concentration of approximately 10^{12} viral particles/ml. To generate EnvA-pseudotyped glycoprotein (G)-deleted rabies virus expressing eGFP (EnvA-RVΔG-eGFP), we followed a published protocol (Osakada and Callaway, 2013). Plasmids expressing the rabies viral components, B7GG, BHK-EnvA and HEK-TVA cells were provided at courtesy of Dr. Edward M. Callaway.

To construct shRNA against Drd3 (Drd3 shRNA), oligonucleotides that contained 21 base-pair sense and antisense sequences (5′-TTCTTCTTGACTCACGTTCTT-3′) targeting Drd3 were connected with a hairpin loop followed by a poly(T) termination signal. This shRNA oligonucleotide was ligated into BLOCK-iT POLII miR RNAi expression vectors (Invitrogen) and then transferred to an AAV vector together with EmGFP. For testing of the efficacy of the shRNA, we stereotaxically injected AAVs expressing Drd3 shRNA into the LS. Two weeks after injection, the virus-infected area labeled EmGFP expression was dissected. Drd3 mRNA levels were measured using quantitative real-time PCR and found to be reduced over 80% (Figures 6G and 6H). To validate the specificity of Drd3 shRNA, a control vector expressing both Drd3 shRNA and shRNA-resistant Drd3 (Drd3*) was cloned (Ma et al., 2007). A mouse

cDNA was amplified by PCR using the following primer sets: Drd3-F: 5′-ATGGCACCTCTGAGCCAGATAAG-3′ and Drd3-R: 5′-TCAGCAGGATAGAATCTTGAGGAAGG-3′. The amplified Drd3 cDNA was inserted into AAV vector to produce AAV-hsyn1-Drd3-eGFP. Site-directed mutagenesis was performed using AAV-hsyn1-Drd3-eGFP as a template to make a shRNA-resistant mutant (Drd3*). Then, this Drd3* cDNA was cloned into AAV vectors expressing Drd3 shRNA to rescue the phenotype induced by knockdown of Drd3.

Stereotaxic Surgeries

Drd3::Cre or wild-type mice (6-12 weeks old) were anesthetized with a mixture of ketamine (100 mg/kg) and dexmedetomidine (0.5 mg/kg). The mouse was mounted in a stereotaxic frame (David Kopf Instruments). Body temperature was kept stable by using a heating pad while recovering from anesthesia. Viral injections were targeted using coordinates based on the Paxinos and Franklin mouse brain atlas (Paxinos and Franklin, 2008). For behavioral or electrophysiology experiments, viral preparations (AAV-DIO-eGFP, AAV-DIO-eGFP-Kir2.1, AAV-EmGFP-Drd3 shRNA, AAV-Drd3*-EmGFP-Drd3 shRNA, AAV-DIO-EmGFP-Drd3 shRNA and AAV-DIO-Drd3*-EmGFP-Drd3 shRNA) in volumes 250-350 nL were injected bilaterally into the LS (bregma, anteroposterior +0.85 mm; lateral ± 0.35 mm; dorsoventral −3.2 mm) or NAc shell (bregma, anteroposterior +1.6 mm; lateral ± 0.5 mm; dorsoventral −4.1 mm) at a slow rate (100 nl/min) using a syringe pump. Mice were allowed 2-3 weeks to recover from the virus injections before starting of behavioral tests. Injection sites were confirmed in all animals by preparing coronal sections containing the desired plane, and animals with an incorrect injection placement were excluded from analyses. For anatomical output mapping, AAV-eGFP or AAV-DIO-eGFP (200 nl) were unilaterally injected into the LS of wild-type or Drd3::Cre mice, respectively. For rabies-mediated retrograde tracing, we first unilaterally injected 200 nL of AAV-DIO-mRuby2-TVA-RVG into the LS of Drd3::Cre mice. Two weeks later, mice were injected with EnvA-RVΔG-eGFP into the LS. All mice were sacrificed 1-2 weeks after the last injection for circuit mapping analysis. For *in vivo* Ca^{2+} imaging experiments, Drd3::Cre animals received the unilateral injection of AAV-DIO-GCaMP6f (250 nl) into the LS. Two weeks later, the snap-in imaging cannula (Model L-V; 500 μm diameter; 5.66 mm length; Doric Lenses) with guiding gradient-index (GRIN) lens was implanted above the previous injection site. The target depth of the lens was adjusted (~100 μm above injection site) by observing fluorescent signals through a snap-in fluorescence microscope body (Doric Lenses). The implanted imaging cannula and focusing ring were secured to the skull with an initial layer of adhesive cement (C&B metabond; Parkell) followed by a second layer of dental cement (Ortho-Jet; Lang). *In vivo* Ca^{2+} imaging tests were performed 3 weeks after the implantation of the image cannula. For optogenetic stimulation of $Drd3^{LS}$ neurons, Drd3::Cre animals were bilaterally injected with 350 nL of AAV-DIO-eYFP or AAV-DIO-ChR2-eYFP into the LS. Bilateral chronic optic fibers (200 μm diameter, 0.22 NA; Doric Lenses) were implanted with the tip ~200 μm above the virus injection site. Implanted fibers were adhered to the skull with adhesive and dental cement as described above. Lastly, sutures or sterile tissue adhesive (Vetbond; 3M) were used to close the incision. For microinjection of the Drd3 agonist into the LS, a guide cannula (26 gauge, 5 mm long; Plastics One) was chronically implanted in this brain region (bregma, anteroposterior +0.85 mm; lateral ± 0.35 mm; dorsoventral −2.7 mm). Implanted cannulae were secured to the skull as described above, and then obturators were placed in the guide cannulae. Behavioral testing was performed 2 weeks after the implantation. Upon completion of all behavioral experiments, viral injections or fiber/cannula placements were confirmed.

Optogenetic Stimulation

A 3-m-long fiber-optic patch cord (Doric Lenses) was connected to the chronically implanted optic fiber and suspended above the behavioral testing area to allow animals to move freely while receiving laser stimulations. The patch cord was connected to a 473-nm laser (OEM Laser Systems). For $Drd3^{LS}$ neuronal stimulation, bilateral activation using ChR2 was achieved by delivering blue light in a high-frequency train (5 ms pulses of 20 Hz; 10-15 mW at tips). For the three-chamber test, each mouse was subjected to the test twice, separated by 24 h, with one session (10 min) paired with optical stimulation (ON) and one with no stimulation (OFF). Similarly, each mouse underwent two reciprocal social interaction tests separated by 24 h, with one of the sessions (5 min) paired with optical stimulation (ON) and one without (OFF). A novel social stimulus was used for each session and groups were counterbalanced for order of light stimulation (Felix-Ortiz and Tye, 2014). For the USV test, the blue light stimulations were delivered to each mouse in a new cage for 5 min, once a day over 3 consecutive days. One hour after the last stimulation, mice were subjected to the USV test.

In Vivo Ca^{2+} Imaging in Freely Moving Mice and Data Analysis

Mice were habituated to an open field arena (44 × 44 × 44 cm^3) with the head-mounted microscope body attached to the top of the imaging cannula for 30 min. Images were acquired at 8 frames per second with an average exposure time of 125 ms using Doric Neuroscience Studio software (version 4.0.1; Doric Lenses). LED power was maintained at 30% with analog gain 2. To examine Ca^{2+} dynamics in response to a social stimulus or a novel object, either a conspecific stranger mouse or a fake mouse (mouse toy) was introduced to the open filed arena after 10 min-recording of baseline fluorescence. Animal behaviors were recorded by a web camera concurrently. This experimental setting was also combined with the USV testing, which allowed the analysis for correlation of neural activity with vocal communications in response to a female mouse. To test whether the Ca^{2+} activity of individual neurons was altered by PD128907 injection, the rate of Ca^{2+} transients observed per min was measured during 5-min periods after PD128907 injection (at 20, 50, 100, and 120 min post-injection) and compared to the rate during a 5-min pre-injection period. All image analyses were performed with a Doric Neuroscience Studio software (Doric Lenses) and custom MATLAB-based software (Mathworks). To remove movement artifacts, individual image frames were aligned using a single frame as a reference, and then

background fluorescence was removed from the aligned images. Regions of interest (ROI) corresponding to cell bodies were determined using an automated cell-finding function and were visually inspected to ensure accuracy. $\Delta F/F_0$ was calculated as $(F-F_0) / F_0$, where F_0 was the lowest 5% of the fluorescence signal for the imaging session being analyzed. To detect individual Ca^{2+} transients, we first processed the $\Delta F/F_0$ time series to remove slow drifts, estimated by a median filter of a 10 s width. Next, median absolute deviation (MAD) of the entire time series was computed. Ca^{2+} transients were extracted by sequentially detecting each upward transient that exceeded a 6-MAD threshold (equivalent to 4-σ assuming normal distribution) and following the previous event by an interval no shorter than 2 s (Calipari et al., 2016).

Slice Electrophysiology Recordings

Coronal slices (300 μm) containing the LS were prepared using a vibratome (Leica VT1200S), in a solution containing (in mM): 110 choline chloride, 25 $NaHCO_3$, 1.25 NaH_2PO_4, 2.5 KCl, 7 $MgCl_2$, 25 glucose, 0.5 $CaCl_2$, 11.6 ascorbic acid, and 3.1 pyruvic acid, saturated with 95% O_2/5% CO_2. Slices were then allowed to recover at 30°C for 20 min, and subsequently at room temperature, in a solution containing (in mM): 118 NaCl, 26 $NaHCO_3$, 11 glucose, 15 HEPES, 2.5 KCl, 1.25 NaH_2PO_4, 2 pyruvic acid, 0.4 ascorbic acid, 2 $CaCl_2$, and 1 $MgCl_2$, saturated with 95% O_2/5% CO_2. Following > 1.5 h of recovery, slices were transferred to a recording chamber perfused with (in mM): 119 NaCl, 26.2 $NaHCO_3$, 11 glucose, 2.5 KCl, 1 NaH_2PO_4, 2.5 $CaCl_2$, and 1.3 $MgCl_2$, saturated with 95% O_2/5% CO_2, and delivered at 2 mL/min at 30 ± 1°C. Whole cell patch clamp recordings were obtained under visual guidance by differential interference microscopy (Olympus BX61WI), using borosilicate glass pipettes (3-4 MΩ) filled with (in mM): 115 $CsMeSO_3$, 1.5 $MgCl_2$, 1 EGTA, 10 HEPES, 4 Mg-ATP, 0.3 Na_3-GTP, 10 Na-phosphocreatine, 2 QX-314, and 10 BAPTA-Cs_4 for all voltage clamp recordings, except mIPSCs, in which case the internal solution consisted of 125 CsCl, 8 NaCl, 0.6 EGTA, 10 HEPES, 4 Mg-ATP, 0.3 Na_3-GTP, 10 Na-phosphocreatine, and 2 QX-314. For current clamp recordings the pipette internal solution consisted of (in mM): 125 K-gluconate, 4 NaCl, 10 HEPES, 0.5 EGTA, 20 KCl, 4 Mg-ATP, 0.3 Na_3-GTP, and 10 Na-phosphocreatine. Liquid junction potentials were left uncompensated. Signals were amplified and filtered (2 kHz) using an Axopatch 700B amplifier, sampled at 10 kHz using a Digidata 1550, and recorded with Clampex (Molecular Devices). Excitatory to inhibitory ratios were calculated as the peak synaptic response at $V_h = -70$ mV divided by the peak synaptic response at $V_h = 0$ mV. Similarly, AMPA to NMDA ratios were calculated as the peak synaptic response at $V_h = -70$ mV divided by the peak synaptic response at $V_h = +40$ mV, with 100 μM picrotoxin added to the external solution. Miniature postsynaptic currents were recorded in the presence of 0.5 μM tetrodotoxin, in addition to either 100 μM picrotoxin for mEPSCs or 10 μM NBQX for mIPSCs. Rheobase was determined as the minimal current step eliciting at least one action potential, using 10 pA increments of 500 ms duration. Analyses were performed offline using Clampfit (Molecular Devices). Only cells with a stable access resistance of < 25 MΩ throughout the recording period were included in the analysis.

Drugs

(+)-PD 128907 hydrochloride (PD128907, Tocris Bioscience) was dissolved in sterile saline. For behavioral experiments, PD128907 (0.5 mg/kg, i.p.) or saline were administered as a series of triple injections 24, 6 and 1 h before the behavioral test. In the experiments for analyzing c-*fos* levels, mice received PD128907 (0.1 or 0.5 mg/kg, i.p.; 0.1 or 2.5 μg/side) or saline 1 h before transcardial perfusion. For electrophysiology experiments, 10 mM PD128907 was diluted to a final concentration of 10 μM in aCSF. Fluoxetine (Sigma-Aldrich) was dissolved in sterile saline. Mice received 14 daily injections of fluoxetine (20 mg/kg, i.p.).

Intracranial Drug Injection and Histology

On the day of the intracranial injection, an internal cannula (33 gauge, projecting 0.5 mm below the tip of the guide; Plastics One) connected to 1 μL syringes (Hamilton) via polyethylene (PE)-20 tubing was inserted into the guide. PD128907 (0.5 or 2.5 μg/side) or saline was microinjected bilaterally into the LS 1 h before behavioral testing. Upon completion of behavioral experiments, mice were anesthetized and perfused with 4% PFA. Brains were extracted and further post-fixed in 4% PFA. Coronal sections (50 μm) were subsequently stained with 0.2% cresyl violet (Sigma-Aldrich) for verification of cannula tip placements. Only mice with injection cannula tips located bilaterally in the LS were included in the data analyses.

QUANTIFICATION AND STATISTICAL ANALYSIS

All statistical analyses were performed with SigmaStat software (version 3.5; Aspire Software). Differences across more than two groups were analyzed with one-way or two-way analyses of variance (ANOVA) followed by Bonferroni or Fisher LSD post hoc tests for multiple comparisons. For comparisons between two groups, Two-tailed t tests (paired or unpaired) or Mann-Whitney *U*-test were used as described in the figure legends. The distribution of data was checked for normality and equal variance. $p < 0.05$ was considered statistically significant. Data are reported as mean ± SEM.

Neuron, Volume *97*

Supplemental Information

Drd3 Signaling in the Lateral Septum Mediates Early Life Stress-Induced Social Dysfunction

Sora Shin, Horia Pribiag, Varoth Lilascharoen, Daniel Knowland, Xiao-Yun Wang, and Byung Kook Lim

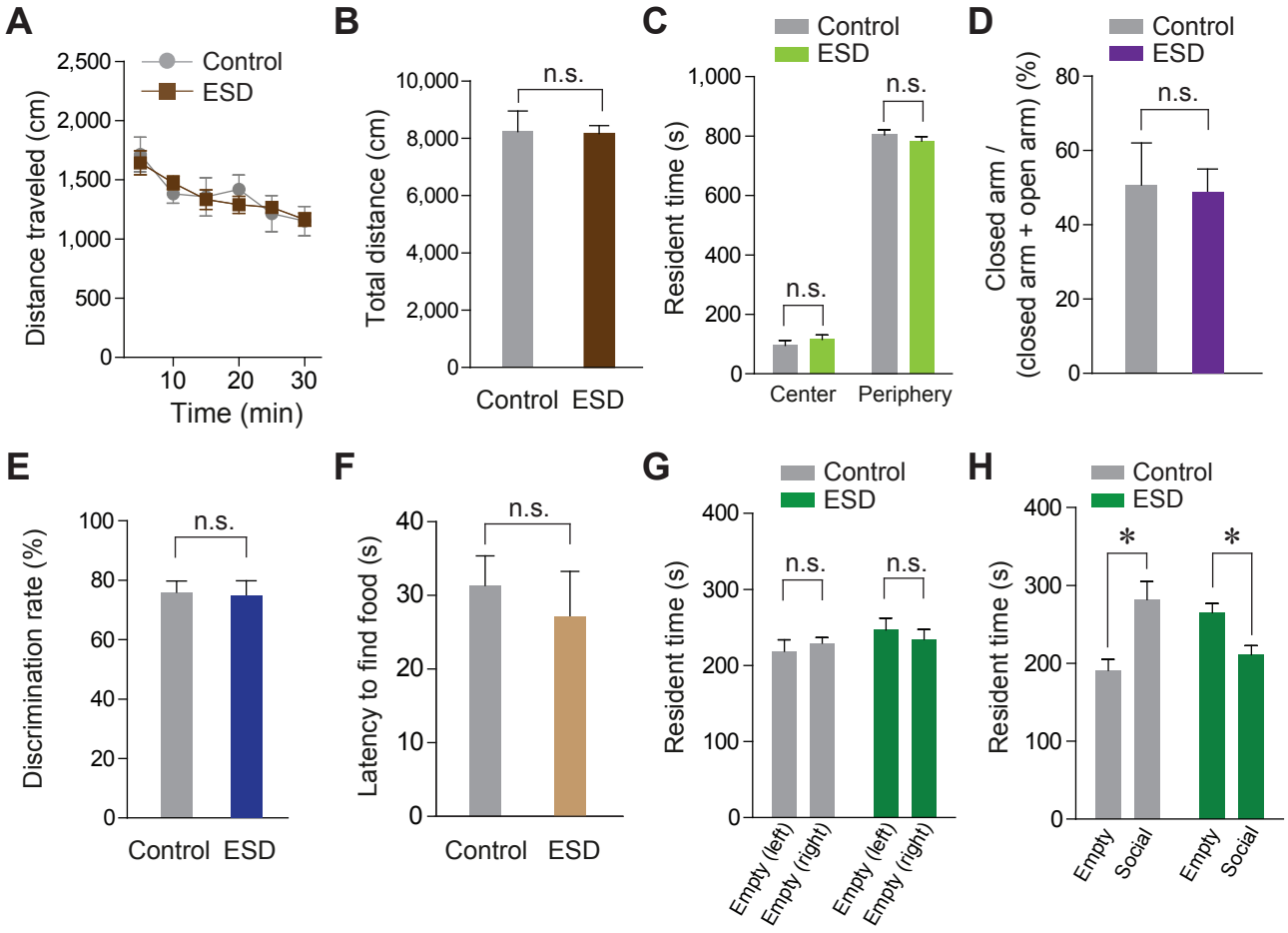
A
Distance traveled (cm)
2,500
2,000
1,500
1,000
500
0
Control
ESD
10
20
30
Time (min)
B
Total distance (cm)
10,000
8,000
6,000
4,000
2,000
0
n.s.
Control
ESD
C
Resident time (s)
1,000
800
600
400
200
0
Control
ESD
n.s.
n.s.
Center
Periphery
D
Closed arm / (closed arm + open arm) (%)
80
60
40
20
0
Control
ESD
n.s.
E
Discrimination rate (%)
100
80
60
40
20
0
n.s.
Control
ESD
F
Latency to find food (s)
40
30
20
10
0
n.s.
Control
ESD
G
Resident time (s)
400
300
200
100
0
Control
ESD
n.s.
n.s.
Empty (left)
Empty (right)
Empty (left)
Empty (right)
H
Resident time (s)
400
300
200
100
0
Control
ESD
*
*
Empty
Social
Empty
Social

Figure S1

Figure S1. Basic Characteristics of ESD mice, Related to Figure 1

(A and B) Locomotor activity was monitored for 30 min and analyzed in 5 min-bins (A) and total distance traveled was measured during the 30 min test period (B). No significant difference in locomotion was observed between control and ESD mice (n = 5 per group).

(C) The resident time spent in the center or periphery of the open field. ESD mice showed normal levels of anxiety-like behaviors comparable to control mice in the open field test (n = 9, 11 mice per group).

(D) Percentage time spent in the closed arms of elevated plus-maze. ESD mice had no observable anxiety in the elevated plus maze (n = 4, 6 mice per group).

(E) Novel object recognition test. ESD mice showed the regular ability to recognize a novel object (n = 9 per group).

(F) Buried food olfactory test. No significant difference in latency to find buried food was observed between control and ESD mice (n = 9, 8 mice per group).

(G) The habituation session of three-chamber test. No side preference was apparent during the habitation for control and ESD mice (n = 7, 11 mice per group).

(H) The test session of three-chamber test. Control mice spent more time in the side designated as the ‘social’ than the ‘empty’ compartment, whereas ESD mice did not show preferences for social compartment (n = 7, 11 mice per group).

Significance for multiple comparisons: Paired *t*-test [(H)], $*P < 0.05$. n.s., not significant. Data are presented as mean ± s.e.m.

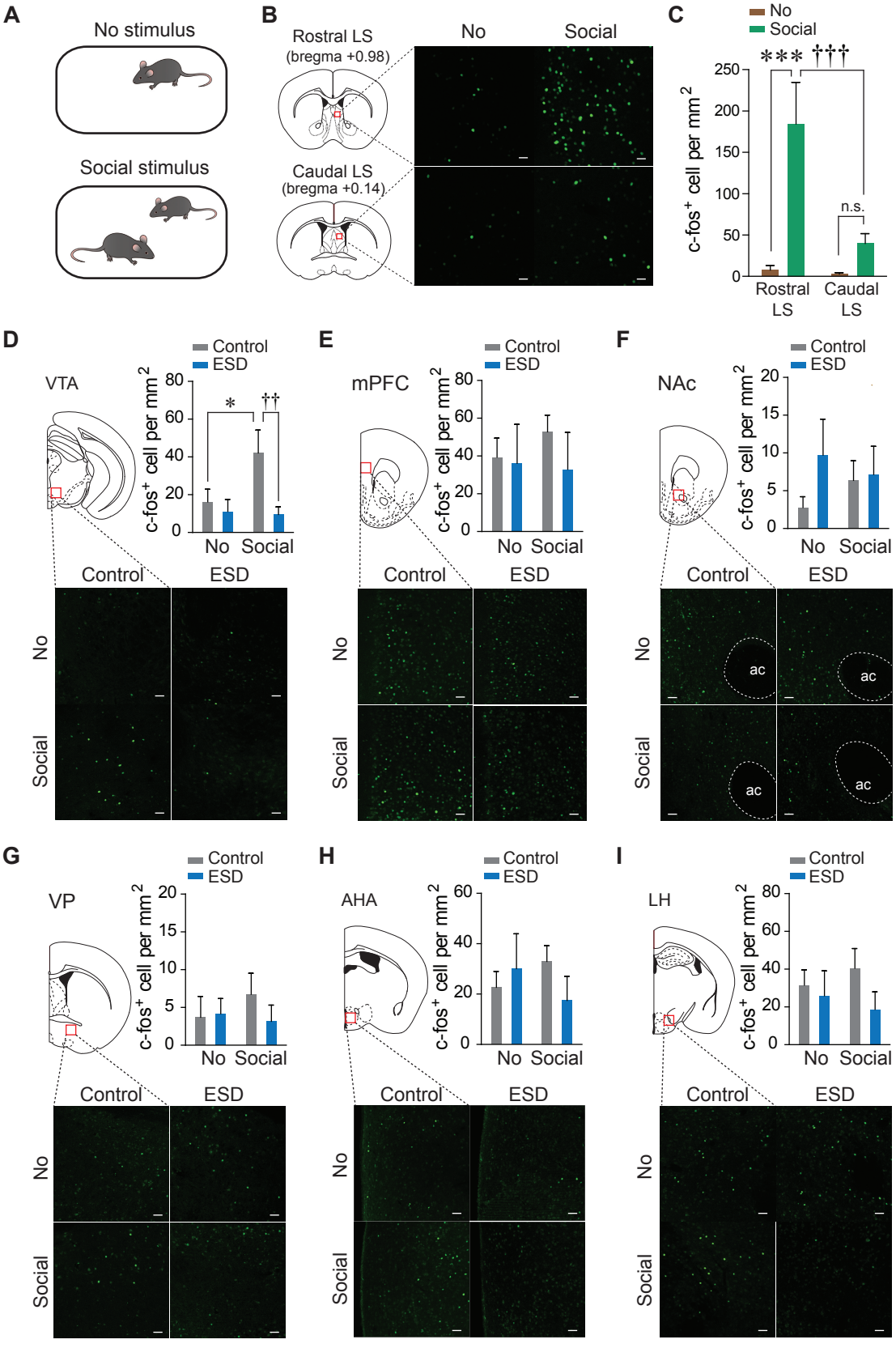
A
No stimulus
Social stimulus
B
Rostral LS
(bregma +0.98)
Caudal LS
(bregma +0.14)
No
Social
C
No
Social
***
†††
n.s.
c-fos+ cell per mm2
Rostral LS
Caudal LS
D
VTA
Control
ESD
*
††
No
Social
E
mPFC
F
NAc
ac
G
VP
H
AHA
I
LH

Figure S2

Figure S2. Quantification of c-fos-positive Cells in the Several Brain Areas Following Exposure to Social Stimulus, Related to Figure 1

(A) Schematics illustrating the experimental design for examining c-fos induction by social stimulus.

(B) Representative images of the rostral and caudal LS of control mice showing c-fos expression following exposure to a social stimulus. Scale bars, 20 μm.

(C) Quantifications of c-fos-positive cells in the rostral and caudal LS. Social stimulus elicited a robust increase of c-fos expression in the rostral LS compared to the caudal LS (n = 6 mice for each no stimulus group and n = 5 mice for each social stimulus group).

(D to I) Quantifications (top) and representative images (bottom) of c-fos-positive cells in the VTA (D), mPFC (E), NAc (F), VP (G), AHA (H) and LH (I) between control and ESD mice after exposure to a social stimulus. Social stimulus induces a robust c-fos expression in the VTA (D) of control, but not of ESD mice (n = 6 mice for each no stimulus group and n = 7 mice for each social stimulus group). No changes in c-fos-positive cells within the mPFC, NAc, VP, AHA and LH. Scale bars, 50 μm. ac, anterior commissure.

Significance for multiple comparisons: Two-way RM ANOVA; post-hoc, Fisher LSD [(C)], and Two-way ANOVA; post-hoc, Bonferroni [(D)], $^{*}P < 0.05$; $^{***}P < 0.001$; $^{\dagger\dagger}P < 0.01$; $^{\dagger\dagger\dagger}P < 0.001$; n.s., not significant. Data are presented as mean ± s.e.m.

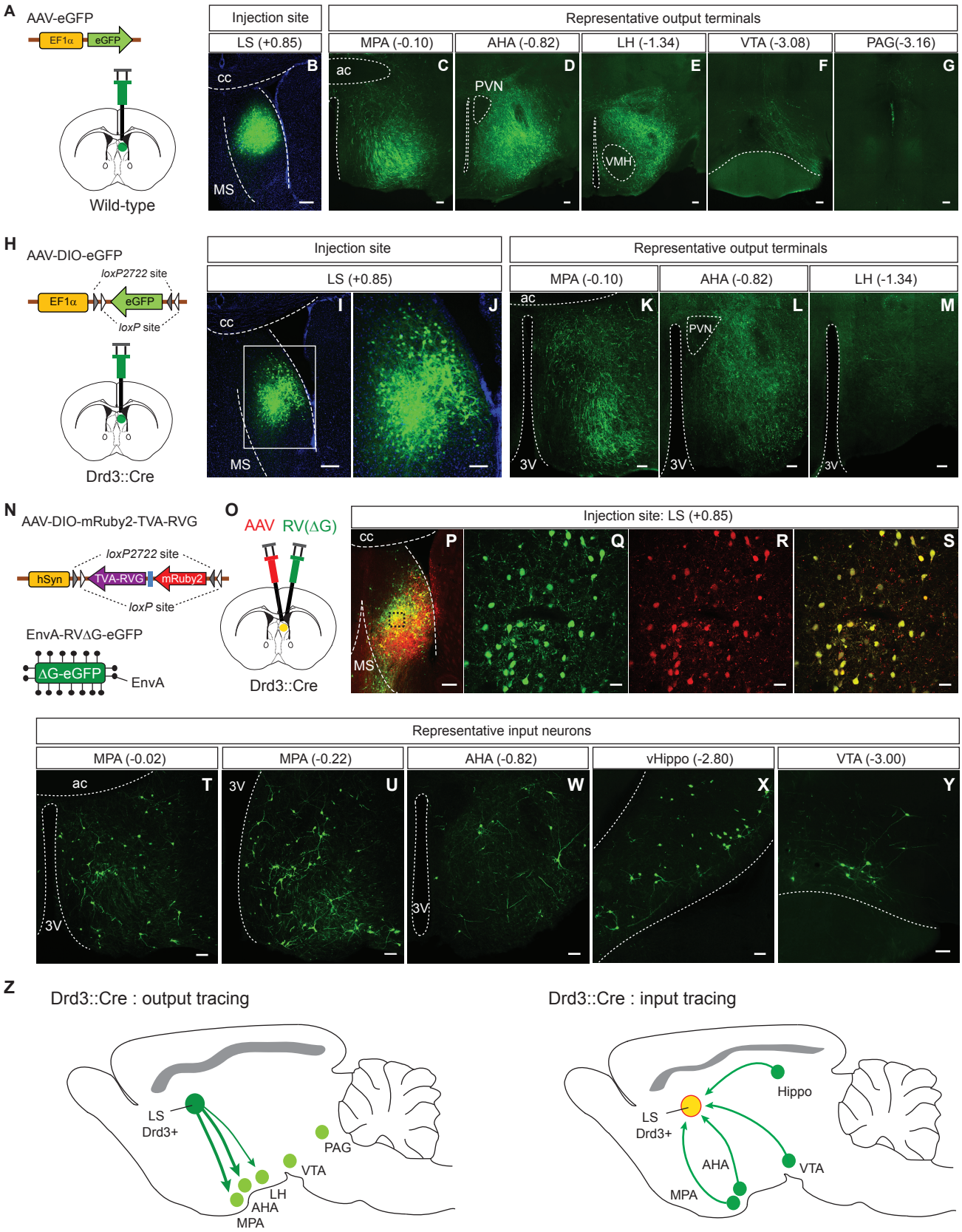
A
AAV-eGFP
EF1α
eGFP
Wild-type
Injection site
Representative output terminals
LS (+0.85)
MPA (-0.10)
AHA (-0.82)
LH (-1.34)
VTA (-3.08)
PAG(-3.16)
B
C
D
E
F
G
cc
MS
ac
PVN
VMH
H
AAV-DIO-eGFP
loxP2722 site
EF1α
eGFP
loxP site
Drd3::Cre
Injection site
Representative output terminals
LS (+0.85)
MPA (-0.10)
AHA (-0.82)
LH (-1.34)
I
J
K
L
M
cc
MS
ac
3V
PVN
N
AAV-DIO-mRuby2-TVA-RVG
loxP2722 site
hSyn
TVA-RVG
mRuby2
loxP site
EnvA-RVΔG-eGFP
ΔG-eGFP
EnvA
O
AAV RV(ΔG)
Drd3::Cre
Injection site: LS (+0.85)
P
Q
R
S
cc
MS
Representative input neurons
MPA (-0.02)
MPA (-0.22)
AHA (-0.82)
vHippo (-2.80)
VTA (-3.00)
T
U
W
X
Y
ac
3V
Z
Drd3::Cre : output tracing
LS
Drd3+
PAG
VTA
LH
AHA
MPA
Drd3::Cre : input tracing
Hippo
LS
Drd3+
AHA
VTA
MPA

Figure S3

Figure S3. The Afferent and Efferent Connections of Drd3^{LS} neurons, Related to Figure 2

(A) Schematic illustrating the injection of AAV expressing eGFP into the LS of wild-type mice.

(B) The image shows a robust eGFP expression in the LS cell bodies without cell-type specificity. Scale bar, 200 μm. cc, corpus callosum; MS, medial septum.

(C to G) eGFP-positive axons from LS cell bodies were found in the MPA (C), AHA (D), LH (E), VTA (F), and PAG (G). Scale bars, 100 μm. ac, anterior commissure; PVN, paraventricular nucleus; VMH, ventromedial hypothalamus.

(H) Schematic illustrating the injection of AAV expressing eGFP in a Cre-dependent manner into the LS of Drd3::Cre mice.

(I and J) The image showing robust eGFP expression in the Drd3^{LS} neuronal cell bodies (I), and its high magnification image (J). Scale bars, 200 μm, 100 μm, respectively.

(K to M) eGFP-positive axons from Drd3^{LS} cell bodies were found in the MPA (K), AHA (L), and LH (M). Scale bars, 100 μm. PVN, paraventricular nucleus; 3V, third ventricle.

(N and O) Schematic showing the strategy for rabies-mediated retrograde tracing of monosynaptic inputs to Drd3^{LS} neurons. Two different viruses were used. AAV expressing both EnvA receptor (TVA) and rabies virus glycoprotein (RVG) in a Cre-dependent manner (AAV-DIO-mRuby2-TVA-RVG); EnvA-pseudotyped glycoprotein (G)-deleted rabies virus expressing eGFP (EnvA-RVΔG-eGFP) (N). AAV-DIO-mRuby2-TVA-RVG was firstly injected into the LS of Drd3::Cre mice. Two weeks later, EnvA-RVΔG-eGFP was injected again into the same site (O).

(P) The confocal image showing starter cells (yellow, expressing both eGFP and mRuby2) in the LS of Drd3::Cre mice. Scale bar, 200 μm.

(Q to S) Enlarged views of a region in the black dotted box showing in (P). Green, expressing eGFP (Q); Red, expressing mRuby2 (R); Yellow, expressing both eGFP and mRuby2 (S). Scale bars, 30 μm.

(T to Y) Images showing rabies-labelled presynaptic neurons in the rostral and caudal part of MPA (T and U, respectively), AHA (W), vHippo (X), and VTA (Y). Scale bars, 100 μm.

(Z) Schematic summary of the brain regions that receive $Drd3^{LS}$ neuronal projections (left) and that provide inputs to $Drd3^{LS}$ neurons (right).

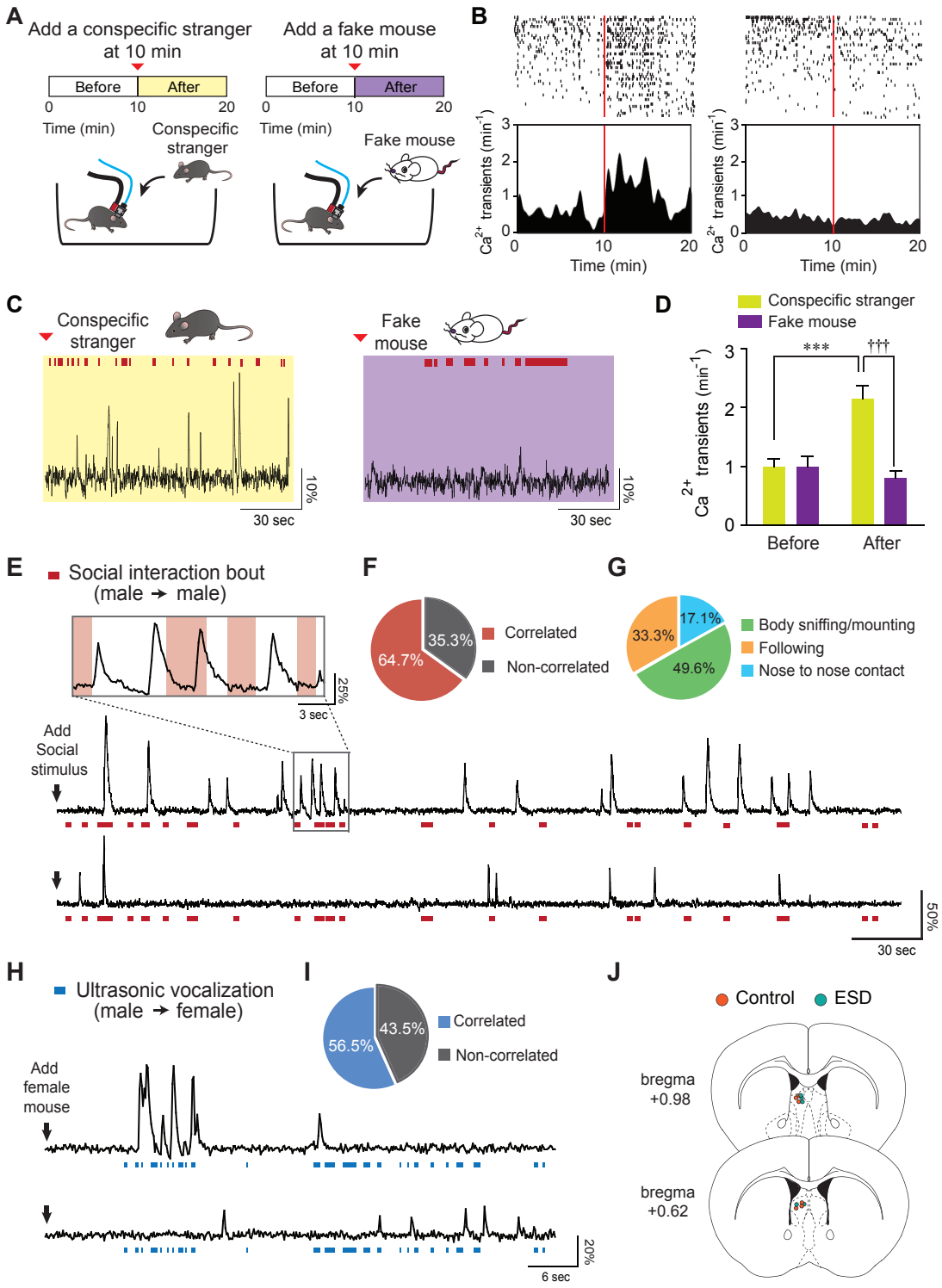
A
Add a conspecific stranger at 10 min
Before
After
0
10
20
Time (min)
Conspecific stranger
Add a fake mouse at 10 min
Before
After
0
10
20
Time (min)
Fake mouse
B
Ca2+ transients (min-1)
3
2
1
0
0
10
20
Time (min)
Ca2+ transients (min-1)
3
2
1
0
0
10
20
Time (min)
C
Conspecific stranger
10%
30 sec
Fake mouse
10%
30 sec
D
Conspecific stranger
Fake mouse
***
†††
Ca2+ transients (min-1)
3
2
1
0
Before
After
E
Social interaction bout (male → male)
25%
3 sec
Add Social stimulus
50%
30 sec
F
35.3%
64.7%
Correlated
Non-correlated
G
17.1%
33.3%
49.6%
Body sniffing/mounting
Following
Nose to nose contact
H
Ultrasonic vocalization (male → female)
Add female mouse
20%
6 sec
I
43.5%
56.5%
Correlated
Non-correlated
J
Control
ESD
bregma +0.98
bregma +0.62

Figure S4

Figure S4. *In vivo* Imaging of Ca^{2+} Dynamics from $Drd3^{LS}$ Neurons of Control Drd3::Cre Mice during Social Interaction, Related to Figure 3

(A) Schematic for *in vivo* imaging of Ca^{2+} dynamics in $Drd3^{LS}$ neurons of control Drd3::Cre mice. Images for fluorescently encoded Ca^{2+} transients were acquired before and after the presentation of either a conspecific stranger (left) or a fake mouse (right).

(B) Raster plots (top) and peristimulus time histograms (bottom) showing $Drd3^{LS}$ neuronal activity of control Drd3::Cre mice in response to either a conspecific stranger (left, n = 44 cells from 3 mice) or a fake mouse (right, n = 48 cells from 4 mice). The rows and ticks in the raster plots represent individual cells and single Ca^{2+} transient events, respectively. Vertical red bars mark the time the conspecific stranger or fake mouse was introduced.

(C) Representative Ca^{2+} activity traces from $Drd3^{LS}$ neurons of control Drd3::Cre mice after presenting of a conspecific stranger (left) or a fake mouse (right), respectively. Red dashed areas indicate physical interaction bouts with a conspecific stranger or a fake mouse.

(D) Normalized average Ca^{2+} transients per min in $Drd3^{LS}$ neurons of control Drd3::Cre mice before and after the presentation of a conspecific stranger or a fake mouse (n = 44 cells from 3 mice for conspecific strangers, n = 48 cells from 4 mice for fake mice).

(E) Example traces of $Drd3^{LS}$ neuronal activity from two representative cells during male to male social interaction. Red dashed areas indicate social interaction bouts. Zoom-in of gray box (top) showed relating GCaMP6f signal of a $Drd3^{LS}$ neuron below with light red shaded areas indicating social interaction.

(F and G) Pie charts indicate percentage of Ca^{2+} transient events from $Drd3^{LS}$ neurons of control Drd3::Cre mice correlating with social interaction bouts (F) and with different subtypes of social interaction behaviors (G) during the first 2 min-recording after introducing a male intruder (n = 33 cells from 3 mice).

(H) Example traces of $Drd3^{LS}$ neuronal activity from two representative cells during USV tests. A female mouse was added for recording USVs produced by male experimental mice. Blue dashed areas indicate the generation of USVs.

(I) Pie charts indicate percentage of Ca^{2+} transient events from $Drd3^{LS}$ neurons of control Drd3::Cre mice correlating with USVs during the first 1-min recording after introducing a female intruder (n = 26 cells from 3 mice).

(J) Locations of the GRIN lens in the Drd3::Cre mice included in Figures 3G to 3J. Symbols represent the different groups: orange circle, control Drd3::Cre mice; blue circle, ESD Drd3::Cre mice.

Significance for multiple comparisons: Two-way RM ANOVA; post-hoc, Fisher LSD [(D)], $^{***}P < 0.001$; $^{\dagger\dagger\dagger}P < 0.001$. Data are presented as mean ± s.e.m.

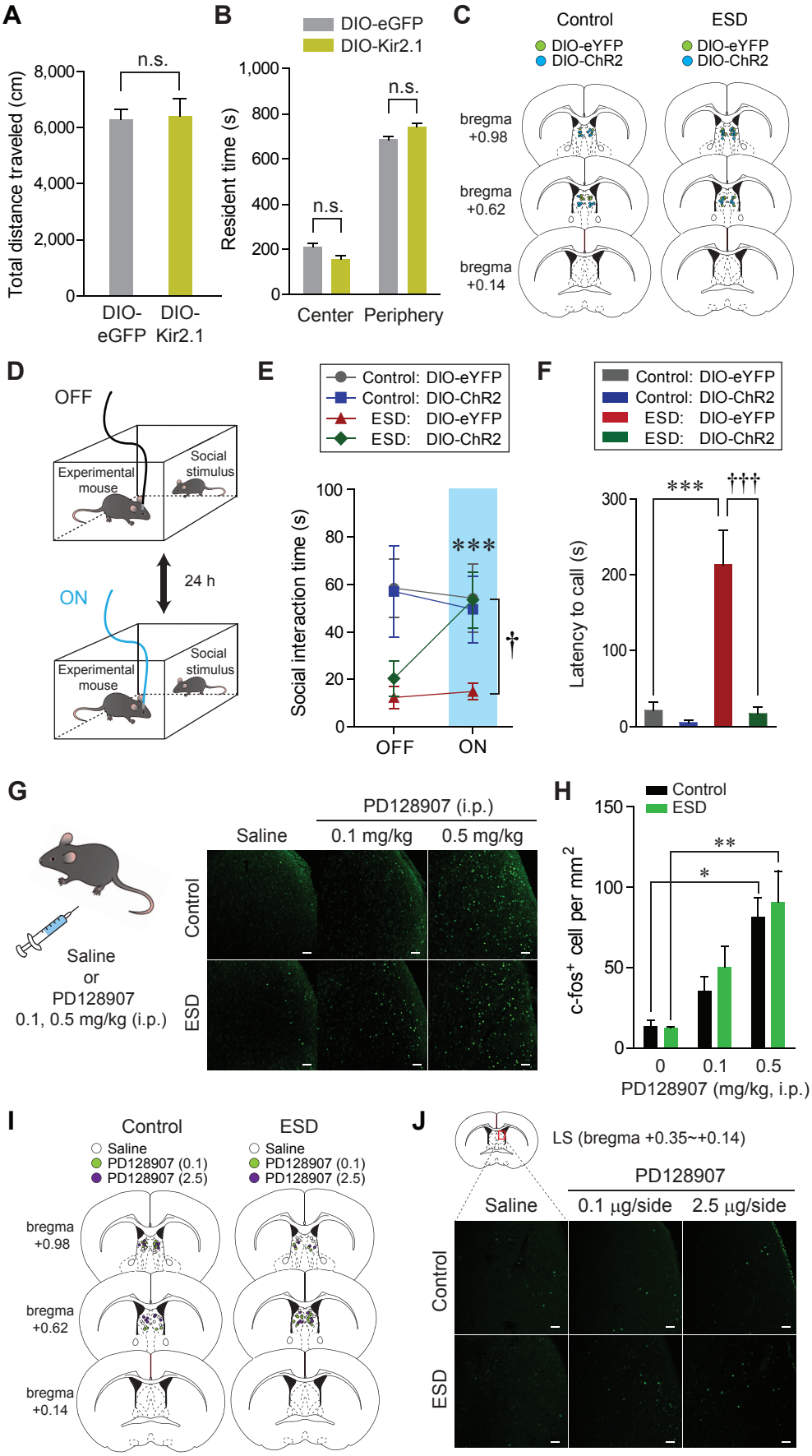
A
Total distance traveled (cm)
8,000
6,000
4,000
2,000
0
n.s.
DIO-eGFP
DIO-Kir2.1
B
DIO-eGFP
DIO-Kir2.1
Resident time (s)
1,000
800
600
400
200
0
n.s.
n.s.
Center
Periphery
C
Control
ESD
DIO-eYFP
DIO-ChR2
DIO-eYFP
DIO-ChR2
bregma +0.98
bregma +0.62
bregma +0.14
D
OFF
Experimental mouse
Social stimulus
24 h
ON
Experimental mouse
Social stimulus
E
Control: DIO-eYFP
Control: DIO-ChR2
ESD: DIO-eYFP
ESD: DIO-ChR2
Social interaction time (s)
100
80
60
40
20
0
***
†
OFF
ON
F
Control: DIO-eYFP
Control: DIO-ChR2
ESD: DIO-eYFP
ESD: DIO-ChR2
Latency to call (s)
300
200
100
0
***
†††
G
Saline
or
PD128907
0.1, 0.5 mg/kg (i.p.)
PD128907 (i.p.)
Saline
0.1 mg/kg
0.5 mg/kg
Control
ESD
H
Control
ESD
c-fos+ cell per mm2
150
100
50
0
**
*
0
0.1
0.5
PD128907 (mg/kg, i.p.)
I
Control
ESD
Saline
PD128907 (0.1)
PD128907 (2.5)
Saline
PD128907 (0.1)
PD128907 (2.5)
bregma +0.98
bregma +0.62
bregma +0.14
J
LS (bregma +0.35~+0.14)
PD128907
Saline
0.1 μg/side
2.5 μg/side
Control
ESD

Figure S5

Figure S5. Modulation of Drd3^{LS} Neuronal Activity affects ESD-induced Abnormal Social Behaviors and Pharmacological Activation of Drd3 signaling Increases LS Neuronal Activity, Related to Figures 4 and 5

(A) Total distance traveled during the 15-min locomotion test. Viral-mediated Kir2.1 expression in the Drd3^{LS} neurons of control Drd3::Cre mice did not alter the locomotion (n = 3, 4 mice per group).

(B) Injection of the AAV-DIO-Kir2.1 into the LS of control Drd3::Cre mice had no effects on anxiety-like behaviors in open field tests (n = 3, 4 mice per group).

(C) Locations of the optic fibers in Drd3::Cre mice included in Figures 4I, 4K. Symbols represent the different groups: light green circle, AAV-DIO-eYFP; blue circle, AAV-DIO-ChR2.

(D) The experimental design of reciprocal social interaction tests with optical stimulations. Five-minutes testing sessions were conducted twice and counterbalanced for order with a 24 h interval between laser ON and laser OFF conditions.

(E) Photoactivation of Drd3^{LS} neurons rescued the amount of time ESD Drd3::Cre mice spent in direct social interaction (sniffing, following, mounting and nose to nose contacts) to the levels of control Drd3::Cre mice (n = 5, 6 mice for each control group and n = 6, 6 mice for each ESD group; ***$P < 0.001$ compared with ESD mice expressing DIO-ChR2 at OFF state; $^{\dagger}P < 0.05$ compared with ESD mice expressing DIO-eYFP at ON state).

(F) Photoactivation of Drd3^{LS} neurons in ESD Drd3::Cre mice restored the latency to make the first USV call (n = 7, 8 mice for each control group and n = 8, 11 mice for ESD group).

(G) Schematics for the intraperitoneal injections of the saline or PD128907 to wild-type mice (left). Representative images of c-fos staining in the LS of control and ESD mice following saline or PD128907 injection (0.1 or 0.5 mg/kg, i.p.). Scale bars, 50 μm (right).

(H) Quantifications of c-fos-positive cells in the LS of control or ESD mice 1 h after saline or PD128907 administration. The high dose of PD128907 activated the LS neurons both in control and ESD mice (n = 3, 4 and 4 mice for each control group and n = 3, 3 and 6 mice for each ESD

group).

(I) Locations of the injection cannula tips in the mice included in Figure 5B. Symbols represent the different groups: white circle, saline; light green circle, PD128907 (0.1 μg/side); purple circle, PD128907 (2.5 μg/side).

(J) Representative images of c-fos immunoreactivity in the caudal LS where cannula tips were not placed. No changes were observed in the c-fos expression levels, regardless of drug treatments.

Significance for multiple comparisons: Two-way RM ANOVA; post-hoc, Fisher LSD [(E)], and Two-way ANOVA; post-hoc, Bonferroni [(F), (H)], $^{*}P < 0.05$; $^{**}P < 0.01$; $^{***}P < 0.001$; $^{\dagger}P < 0.05$; $^{\dagger\dagger\dagger}P < 0.001$. n.s., not significant. Data are presented as mean ± s.e.m.

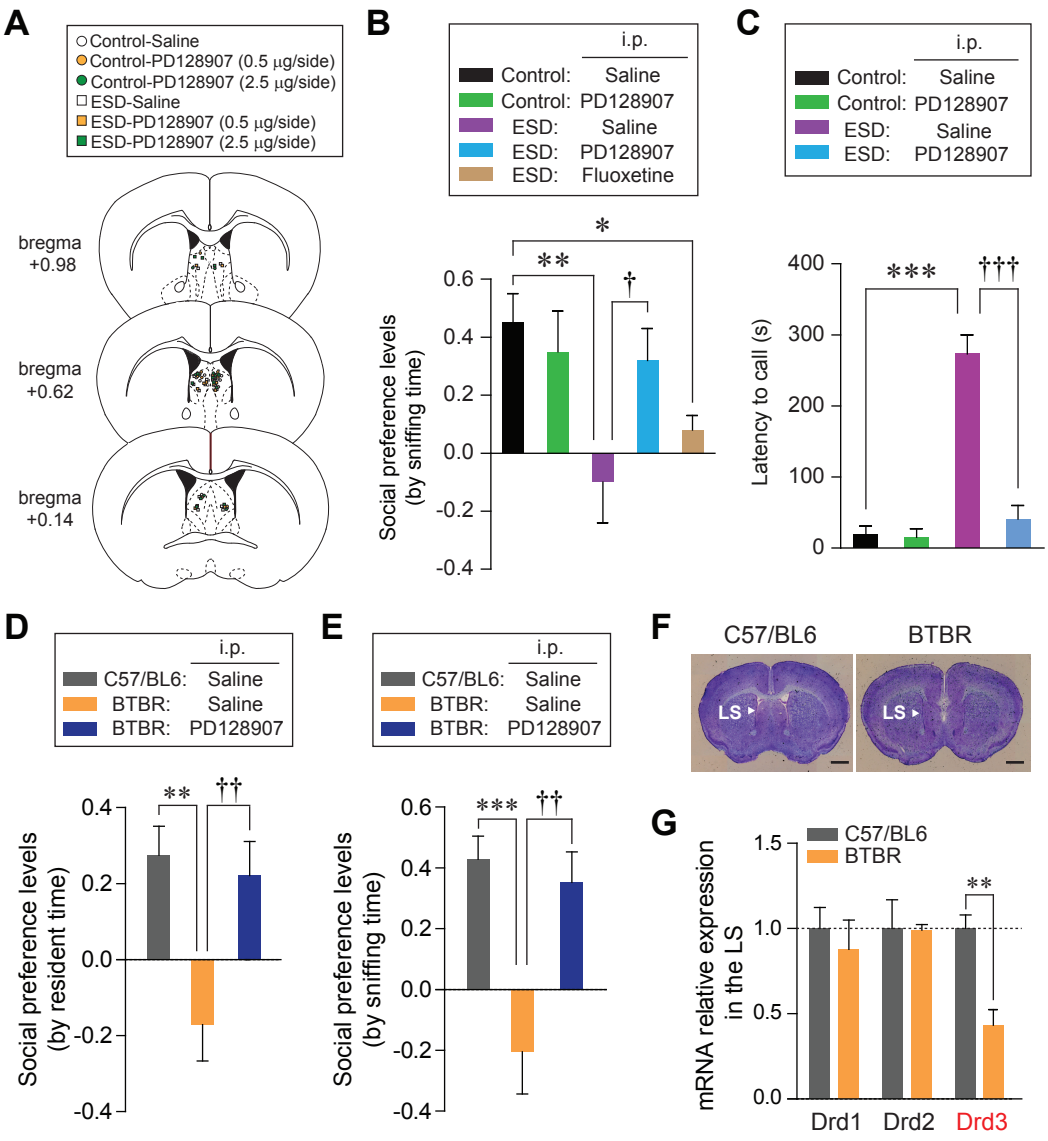
A
Control-Saline
Control-PD128907 (0.5 μg/side)
Control-PD128907 (2.5 μg/side)
ESD-Saline
ESD-PD128907 (0.5 μg/side)
ESD-PD128907 (2.5 μg/side)
bregma +0.98
bregma +0.62
bregma +0.14
B
i.p.
Control: Saline
Control: PD128907
ESD: Saline
ESD: PD128907
ESD: Fluoxetine
Social preference levels (by sniffing time)
C
i.p.
Control: Saline
Control: PD128907
ESD: Saline
ESD: PD128907
Latency to call (s)
D
i.p.
C57/BL6: Saline
BTBR: Saline
BTBR: PD128907
Social preference levels (by resident time)
E
i.p.
C57/BL6: Saline
BTBR: Saline
BTBR: PD128907
Social preference levels (by sniffing time)
F
C57/BL6
BTBR
LS
LS
G
C57/BL6
BTBR
mRNA relative expression in the LS
Drd1
Drd2
Drd3

Figure S6

Figure S6. Administration of Drd3 Agonist, PD128907 (0.5 mg/kg, i.p.) Reverses Social Impairments in both ESD and BTBR mice, Related to Figure 6

(A) Locations of the injection cannula tips in the mice included in Figure 6C. Symbols represent the different groups: white circle, control-saline; yellow circle, control-PD128907 (0.5 μg/side); green circle, control-PD128907 (2.5 μg/side); white rectangle, ESD-saline; yellow rectangle, ESD- PD128907 (0.5 μg/side); green rectangle, ESD-PD128907 (2.5 μg/side).

(B) Social preference levels based on sniffing time in three-chamber test. PD128907 administration rescued impaired social preferences in ESD mice to the level of control mice, whereas chronic fluoxetine did not (n = 6, 5 mice for each control group, n = 6, 6 and 5 mice for each ESD group).

(C) PD128907 administration restored the latency to produce the first USV call emitted by ESD mice (n = 5, 6 mice for each control group, n = 6, 6 mice for each ESD group).

(D and E) PD128907 administration rescued impaired social preference of BTBR mice, a traditional animal model of ASD, based on resident time (D) and on sniffing time (E) in three-chamber test (n = 10 mice for C57/BL6 group, n = 8, 8 mice for each BTBR group).

(F) Representative images of coronal brain slices showing the LS of C57/BL6 (left) and BTBR mice (right). Scale bars, 1 mm.

(G) qRT-PCR analysis of Drd3 mRNA expression from the LS of C57/BL6 versus BTBR mice (n = 5 mice for C57/BL6 group, n = 4 mice for BTBR group).

Significance for multiple comparisons: One-way ANOVA; post-hoc, Fisher LSD [(B), (D), and (E)], Two-way ANOVA; post-hoc, Bonferroni [(C)], and Unpaired t-test [(G)], $*P < 0.05$; $**P < 0.01$; $***P < 0.001$; $^{\dagger}P < 0.05$; $^{\dagger\dagger}P < 0.01$; $^{\dagger\dagger\dagger}P < 0.001$. Data are presented as mean ± s.e.m.

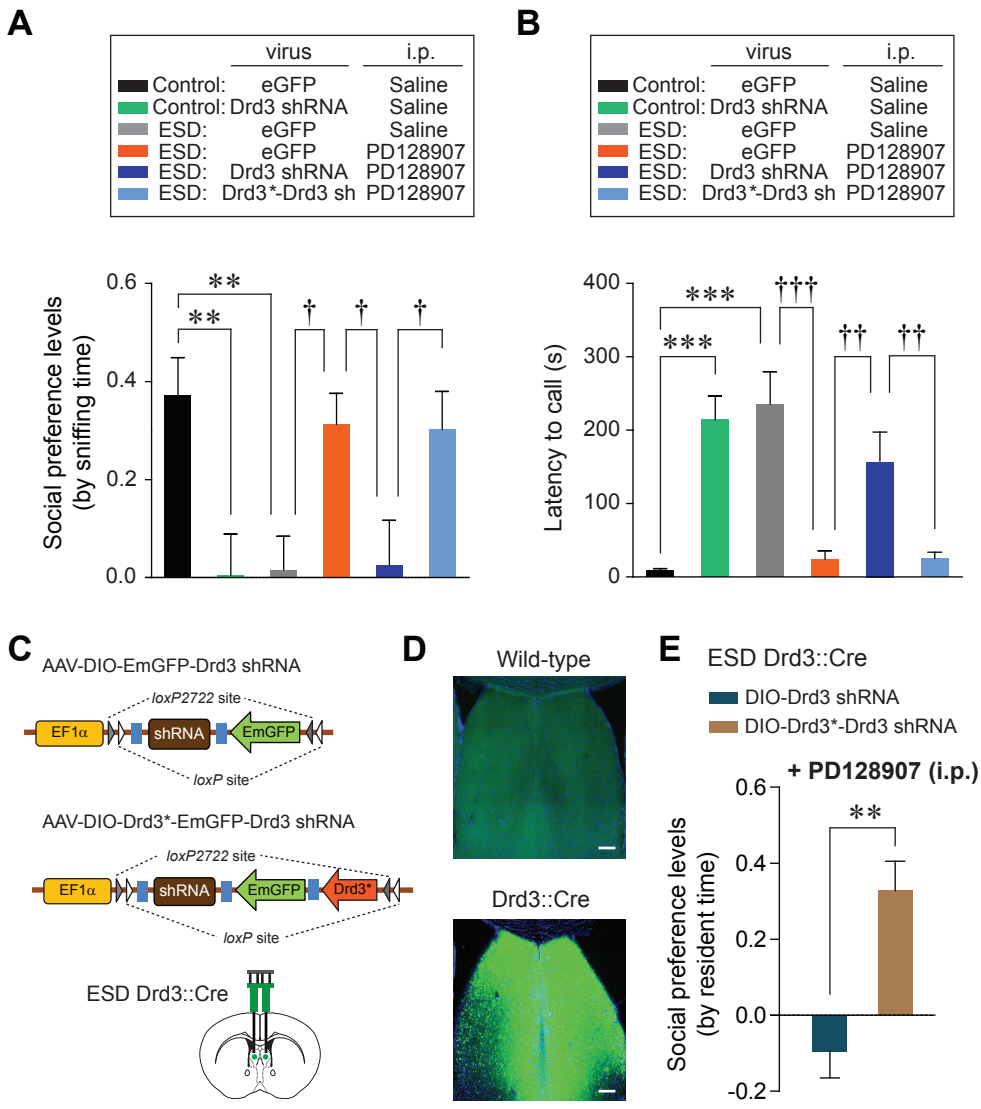
A
virus
i.p.
Control: eGFP Saline
Control: Drd3 shRNA Saline
ESD: eGFP Saline
ESD: eGFP PD128907
ESD: Drd3 shRNA PD128907
ESD: Drd3*-Drd3 sh PD128907
Social preference levels (by sniffing time)
0.6
0.4
0.2
0.0
**
**
†
†
†
B
virus
i.p.
Control: eGFP Saline
Control: Drd3 shRNA Saline
ESD: eGFP Saline
ESD: eGFP PD128907
ESD: Drd3 shRNA PD128907
ESD: Drd3*-Drd3 sh PD128907
Latency to call (s)
400
300
200
100
0
***
***
†††
††
††
C
AAV-DIO-EmGFP-Drd3 shRNA
loxP2722 site
EF1α
shRNA
EmGFP
loxP site
AAV-DIO-Drd3*-EmGFP-Drd3 shRNA
loxP2722 site
EF1α
shRNA
EmGFP
Drd3*
loxP site
ESD Drd3::Cre
D
Wild-type
Drd3::Cre
E
ESD Drd3::Cre
DIO-Drd3 shRNA
DIO-Drd3*-Drd3 shRNA
+ PD128907 (i.p.)
Social preference levels (by resident time)
0.6
0.4
0.2
0.0
-0.2
**

Figure S7

Figure S7. Administration of Drd3 Agonist, PD128907 (0.5 mg/kg, i.p.) Reverses ESD-Induced Social Impairments via Drd3^{LS} Neuronal Signaling, Related to Figure 6

(A and B) Knock-down of Drd3 by injection of AAV-Drd3-shRNA into the LS attenuated social preference levels based on sniffing time in three-chamber test (A) and delayed latency for making the first USV call (B) in control mice. It also blocked PD128907-induced rescue of social dysfunctions in ESD mice. However, the expression of shRNA-resistant Drd3 (Drd3*, mutant form is indicated by asterisk) together with shRNA against Drd3 (AAV-Drd3*-Drd3 sh) did not block PD128907-induced rescue of those social impairments in ESD mice. (A, n = 11, 10 mice for each control group, n = 9, 10, 11 and 11 mice for each ESD group). (B, n = 8, 10 mice for each control group, n = 7, 8, 9 and 10 mice for each ESD group).

(C) Schematic illustrating the bilateral injections of AAV expressing Drd3 shRNA or Drd3*-Drd3 shRNA in a Cre-dependent manner into the LS of ESD Drd3::Cre mice.

(D) Images of the Drd3*-EmGFP-Drd3 shRNA expression after bilateral injections of AAV-DIO-Drd3*-EmGFP-Drd3 shRNA into the LS of wild-type (top) and Drd3::Cre mice (bottom). Scale bars, 250 μm.

(E) Social preference levels based on resident time in three-chamber test. Selective expression of Drd3*-Drd3 shRNA in Drd3^{LS} neurons of ESD Drd3::Cre mice still did not preclude PD128907-induced rescue of impaired social preference (n = 4 mice per group).

Significance for multiple comparisons: One-way ANOVA; post-hoc, Fisher LSD [(A), (B)], Unpaired t-test [(E)], $^{**}P < 0.01$; $^{***}P < 0.001$; $^{\dagger}P < 0.05$; $^{\dagger\dagger}P < 0.01$; $^{\dagger\dagger\dagger}P < 0.001$. Data are presented as mean ± s.e.m.